Thesis for the degree of Licentiate of Engineering

Electron Transport and Collective Modes in Fermi and non-Fermi Liquids

Eric Nilsson

Department of Physics
Chalmers University of Technology
Gothenburg, Sweden 2024

Electron Transport and Collective Modes in Fermi and non-Fermi Liquids
Eric Nilsson

This thesis has been printed using LaTeX.

Department of Physics
Chalmers University of Technology
SE-412 96 Gothenburg
Sweden
Telephone +46 (0)31-7721000

Printed by Chalmers digitaltryck
Gothenburg, Sweden 2024

Electron Transport and Collective Modes in Fermi and non-Fermi Liquids
Eric Nilsson
Department of Physics
Chalmers University of Technology

Abstract

Today's novel materials can display many interesting phases. Two-dimensional materials with strong electron-electron interactions allow the electrons to enter a hydrodynamic regime at intermediate temperatures. This thesis presents a method for an exact description of the quasiparticle distribution in terms of kinetic theory, valid beyond the asymptotic low-temperature regime used in perturbative approaches. This is used to obtain of the full mode spectrum of the interacting electron gas. At low temperatures, the existence of long-lived modes of odd parity hint at the existence of a new transport regime in between the limits of ballistic and hydrodynamic flow. The method is also used to determine the shear viscosity of the electron liquid beyond the low temperature limit.

If the coupling becomes strong enough, it invalidates the quasiparticle picture, which undermines many established methods within many-body physics. This happens in the strange metal phase of high-temperature superconductors, where the holographic duality – providing a description of a strongly coupled theory in terms of a weakly coupled gravitational theory – serves as one of the few ways to study the strongly coupled physics.

Recent experiments on strange metals show an incoherent plasmon at small momenta, in qualitative agreement with previous holographic models of bulk plasmons. However, the relevant experiments also couple to collective surface excitations, which hitherto has not been considered. This thesis also presents a model for surface plasmon polaritons using the holographic duality, improving the theoretical description of plasmons in strongly correlated materials.

Publications

This thesis is based on the work contained in the following papers.

I "Shear viscosity in interacting two-dimensional Fermi liquids"
U. Gran, **E. Nilsson**, J. Hofmann
Preprint: arXiv:2312.09977 [cond-mat.mes-hall]

II "Nonequilibrium relaxation and odd-even effect in finite-temperature electron gases"
E. Nilsson, U. Gran, J. Hofmann
(*in preparation*)

III "Holographic surface plasmon polaritons"
E. Nilsson, U. Gran
(*in preparation*)

Statement of contributions

My contributions to the included papers were:

I I derived the low-temperature analytical results, and performed the comparison against known theoretical results and experimental data. I partook in finalizing the draft together with my co-authors.

II I performed all of the data analysis and produced all of the results and figures. I did all of the analytical calculations and wrote the first draft of the manuscript, finalizing it together with my co-authors.

III I wrote all of the code, performed all simulations and produced all of the figures and numerical results. I came up with the idea on how to formulate the specific combination of boundary conditions and how to obtain a well-behaved response function. I wrote a majority of the draft appended in this thesis.

Acknowledgements

First, I would like to extend my sincere gratitude to my supervisor Prof. Ulf Gran for the guidance, help, and time devoted to me during these projects. You always care about my well-being and I thoroughly enjoy our time together. Furthermore, thank you to Oliver Thim, not only for the useful feedback on this thesis, but also for the many helpful discussions during the last few years. I would also like to thank Prof. Bengt EW Nilsson for his continuous encouragement and for getting me to do the physics that I do. Finally, I would like to send love to my family and my dear Malin. Without you, this effort would mean nothing.

This work was supported by the Area of Advance Nano (formerly Excellence Initiative Nano) at Chalmers University of Technology.

Contents

Chapter 1

Introduction

This thesis covers two different regimes of condensed matter systems. On one side, there are systems with well-defined *quasiparticles*: At low temperatures, the primary excitations responsible for the dynamics of the system are those close to the Fermi surface [1]. This is the basis of Landau's *Fermi liquid theory* [2], which stands as of the most successful theories in physics in the last century.

Although Fermi liquid theory is almost 70 years old, there are still new insights to be gained. Due to the complexity of the governing equations, there is a general notion that "Fermi liquid theory is too hard to solve", and the rise of two-dimensional materials in the last decades has not made the situation any easier. Compared to their three-dimensional counterparts, the lower carrier densities in two dimensions imply a Fermi temperature T_F on the order of 100 K rather than 10^5 K [3]. This means that low-temperature expansions in T/T_F — successful in three dimensions — become much more limited in the two-dimensional world. With many interesting physical phenomena near T_F, such as hydrodynamic behavior of the electrons, there is a need for new methods that can tackle a full solution to the governing equations. This is one of the aspects that we will explore in this thesis.

On the other side, there exists systems with inter-particle correlations so strong, that the quasiparticle lifetime is incredibly short. This can imply a mean free path shorter than the de Broglie wavelength, which is incompatible with the Heisenberg uncertainty relation, and make the quasiparticle concept lose its meaning. The system instead behaves as a strongly correlated electron "soup" [4], and exemplifies *non*-Fermi liquid physics. The strong correlations are problematic for perturbative approaches; for instance, in charge-neutral graphene, the effective coupling constant used in series expansions can exceed unity [5]. Additionally, brute-force simulations of the interacting electrons are greatly hindered by the NP-hard "fermion sign problem" [6] that ruins the con-

vergence of the numerical Quantum Monte Carlo algorithms [7], although some progress has been made on this front in models of quantum critical systems [8].

Since much of the powerful many-body methods rely on the aforementioned quasiparticle concept, an alternative description is needed. Through the use of the *holographic duality*, that we discuss in Chapter 3, a strongly coupled theory admits a dual description in terms of a weakly coupled theory in a higher dimension. The price one pays for the exchange of coupling strengths is the inclusion of gravitational fields in the weakly coupled theory. While Einstein's equations are not trivial, the holographic duality serves as one of the few ways to "solve" a strongly coupled theory, as it is able to generate all n-point correlation functions of the theory with little effort.

The conjectured holographic duality is most precise when applied to systems that at first glance bear little resemblance to those of condensed matter physics. However, the phenomena of interest are explained in terms the low-energy, emergent IR behavior of the theory, and just like many roads lead to Rome, many different UV theories share the same IR fix point. The holographic duality can therefore provide crucial insight through the universal features of strongly correlated systems. Nonetheless, key features of condensed matter systems, such as their thermodynamic properties, the effects of the lattice, and the long-ranged Coulomb interaction, need to be incorporated within the holographic framework in order to make a serious attempt at explaining any experimental data. Many of these effects have been successfully implemented at this point, and in this thesis, we focus on the Coulomb interaction in particular, and discuss the collective modes it gives rise to.

In the end, no realistic system is a perfect Fermi or non-Fermi liquid. Some systems are closer to one end than another, but only through the exploration of physics at both ends might we be able to understand nature.

What are Quasiparticles?

An intuitive description of a quasiparticle is given in Ref. [9]: Consider a horse galloping across a dusty plain. As the horse moves, it spurs up a cloud of dust, and we label the combined object of horse and dust cloud as a *quasihorse*. This quasihorse has different properties than the "naked" horse (e.g., a different mass), and is partly hidden from the environment by the dust cloud. In much the same way, an electron travelling through a material interacts with the surrounding medium, giving it an *effective mass* m^* different from its bare mass, and a finite lifetime τ_{qp}. The validity of the quasiparticle description hinges on $E_{\mathrm{qp}}\tau_{\mathrm{qp}} \gg \hbar$, where E_{qp} the quasiparticle energy [1]. This is satisfied for excitations within a thin shell (of width $\sim T/T_F$) near the Fermi surface, which constrains the low-energy dynamics to excitations with momenta close to the Fermi momentum, k_F. Furthermore, the Coulomb interaction is weakened by the charges in the surrounding medium, just like how the dust cloud hides the

horse. These ideas therefore allow the many-body problem of $\mathcal{O}(10^{23})$ interacting electrons to be recast into that of weakly interacting quasielectrons near the Fermi surface. This describes the behavior of most metals at low temperatures, so notwithstanding the long-ranged nature of the Coulomb interaction, many metals can be considered as weakly correlated systems [10].

The Collisionless-to-Hydrodynamic Crossover

Particularly interesting are materials where electron-electron interactions are dominant. These have become experimentally realizeable due to the development of new fabrication techniques. By layering an electron gas on top of doped material (using so-called modulation doping), the charge carriers become spatially separated from the defects [11]. In effect, this produces very clean materials for which impurity scattering is relevant only at the lowest of temperatures. If the electrons are interacting only amongst themselves, the momentum and energy conservation at the microscopic level translates to the macroscopic level. In this case, the collective behavior of the electrons is like that of a liquid, controlled by hydrodynamics.

A hydrodynamic regime dramatically alters the behavior of the system: With momentum globally conserved, the static conductivity is in principle infinite, where one can imagine the electron fluid flowing around the impurities. In a realistic setting, the electrons flow through a channel or wire of finite width, where momentum is lost due the interactions with the boundaries. The resistivity is therefore determined by the drag along the edges, controlled by the *shear viscosity*, a property of the fluid itself. This is a markedly different from the typical case of ballistic flow, where the resistivity is (among other things) determined by the scattering off impurities and phonons — a property of the environment through which the electrons flow [12]. Hydrodynamic behavior has been reported in mono- [13–18] and bilayer [19] graphene, (Al,Ga)As heterostructures [3, 20–22], GaAs quantum wells [23, 24], $PdCoO_2$ [25] and in Weyl semimetals [26]. Aspects of hydrodynamics, such as shocks or turbulence, could be used in future electronic devices, and through the viscosity, the resistance in nanostructures could go below previously thought fundamental limits [12].

While momentum and energy are only approximately conserved in a realistic setting, hydrodynamic effects become visible when electron-electron interactions provides the dominant equilibration mechanism for the electron gas [27]. As the rate such interactions generally scales as T^2/T_F, the following picture emerges: The temperature must be high enough for electron-electron scattering to dominate the temperature-independent impurity scattering, yet low enough for phonon scattering to be subdominant. Within such a temperature window of electron-electron interaction-dominated transport, the electron fluid can undergo a transition into a hydrodynamic regime, as depicted in Fig. 1.1. If probed at length scales smaller than the characteristic length scale $\ell_{ee} \sim T_F/T^2$

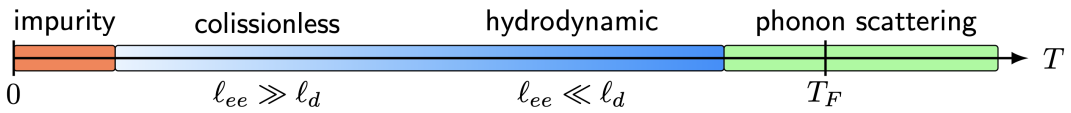

Figure 1.1: Different transport regimes of clean, two-dimensional materials. At low temperatures, impurity scattering dominates; at high temperatures, phonons dominate. In the intermediate regime, dominant electron-electron interactions allow for a crossover between a collisionless and a hydrodynamic regime.

of electron-electron interactions, the system is in a collisionless regime, where excitations are not able to relax efficiently. Conversely, at length scales larger than ℓ_{ee}, the system relaxes quickly, with dynamics dominated by the modes of the (approximately) conserved quantities; energy, momentum, and particle number. Higher temperatures therefore facilitate the transition into the hydrodynamic regime [10]. The restriction to two dimensions is therefore crucial in making T/T_F large before phonons take over, or worse, before the material melts.

Near the Fermi temperature, where hydrodynamic behavior is pronounced, there is a significant brocading of the Fermi surface, lessening the effects of Pauli blocking. The system is therefore neither in the regime where low-temperature approximations are valid, nor is it behaving classically as it does at higher temperatures. There is therefore a need for a complete mathematical description of interacting electrons, valid at all temperatures. This is addressed in paper II, where we present the a method for an exact solution to the kinetic equation describing the two-dimensional electron gas. In paper I, we apply the method to the calculation of the shear viscosity of the electron liquid, valid at all temperatures. An introduction to the papers and a brief highlight of the results are presented in Chapter 2.

Planckian Transport and Holography

The aforementioned hydrodynamic regime is enabled by strong electron-electron interactions. When the interactions become even stronger, the destruction of quasiparticles can lead to non-Fermi liquid behavior, the poster child of which is the *strange metal* phase in cuprate and iron-based high-temperature superconductors (HTS). It is the normal phase out of which superconductivity emerges, placed above the superconducting dome in the phase diagram [28], which is illustrated in Fig. 1.2. Unlike conventional superconductors explained by BCS theory [29], the mechanism underlying superconductivity in HTS is not understood, which adds to the motivation of understanding the strange metal: Since it competes with the superconducting phase, could understanding it hold the

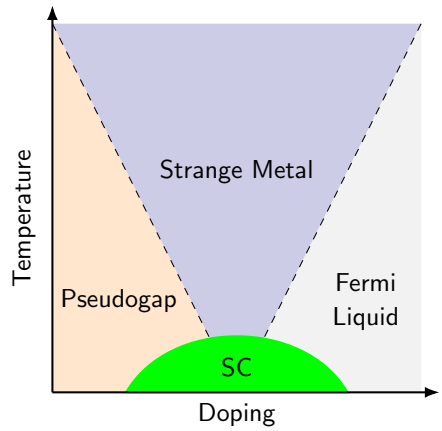

Figure 1.2: Schematic phase diagram of hole-doped high-temperature superconductors [28]. Above the superconducting dome (SC) sits the strange metal phase.

key to unlocking even higher temperature superconductivity?

The prototypical example highlighting the strangeness of the strange metal is the DC resistivity in a HTS at optimal doping[1]. In a normal metal, the quasiparticle-based transport yields a resistivity with a nontrivial temperature dependence, due to the interactions with other quasiparticles. For instance, ballistic electron-electron scattering gives a resistivity proportional to T^2, whereas phonons give a T^5-dependence, that transitions to T-linear around the Debye temperature. Eventually, the mean-free path of the electrons becomes comparable to the lattice spacing, causing the resistivity to saturate. This is the so-called Mott-Ioffe-Regel (MIR) limit, and acts as an upper bound of the resistivity. The situation is very different in a HTS like $La_{2-x}Sr_xCuO_4$ at optimal doping. Here, the resistivity above the superconducting transition temperature T_c increases linearly with temperature in an almost perfect straight line [30], which signals that there is other physics at play [4]. Perhaps even more surprising is that the resistivity shoots right through the MIR limit and keeps growing linearly, in principle until the material melts[2]. Quasiparticles cannot be the primary charge carriers above the MIR limit, and since the resistivity curve shows no sign of changing passing through it, the same could also be true below the MIR limit [31]. The simple behavior of the straight line would "need a powerful mechanism to protect it", in the words of Nobel laureate Bob Laughlin [4]. Understanding this mechanism could allow for the engineering of materials that

[1] This is where the superconducting transition temperature T_c is the largest.

[2] Metals that violate the MIR limit are called *bad metals* in the regime above the limit.

are superconducting at even higher temperatures, as the linear-in-T slope seems to be related to T_c [31].

Measurements of the optical conductivity, $\sigma(\omega)$, reveals another surprising feature [32]. Using the Drude formula of the conductivity to extract a relaxation time τ (which admittedly might be inappropriate to do), one finds it to be very small: In fact, it comes close to the *Plackian timescale*[3] [33],

$$\tau_{\mathrm{pl}} = \frac{\hbar}{k_B T} \tag{1.1}$$

where k_B is Boltzmann's constant and T the temperature. This acts as the shortest possible time of heat loss in a quantum many-body system [34], and is the elementary quantity of dimension time for a quantum system at finite temperature. The Planckian timescale, that also can be inferred from the T-linear resistivity [35], is associated with a highly entangled many-body state, and signals that the charge carriers need not be interpreted as particles [31].

Intriguingly, τ_P is also the relaxation time of black holes, which in part has motivated the effort of modeling strange metals using the holographic duality [36]. As we will see in Chapter 3, the low-energy physics of the strongly correlated theory is indeed captured by black hole dynamics in the gravitational theory. Holographic models of strange metals are a promising candidate [37], and recent models are able to feature both a T-linear resistivity and to reproduce certain aspects of the optical conductivity data [38]. It is however not only the T-linear resistivity or optical conductivity that is a conundrum, but rather the combination with other anomalous measurements, such as a Hall angle $\cot\Theta_H \sim T^2$ [31]. Models that can capture all of the peculiar features of strange metals are under intense pursuit. Whether the prevailing theory will turn out to be a holographic model or something else (see, e.g., [39]), only time will tell.

Collective Modes in Strange Metals

The story of experiments on strange metals with anomalous outcomes is long. Of particular interest in this thesis is the density-density response, as measured by momentum-resolved electron energy loss spectroscopy (M-EELS). It exhibits a very broad plasmon peak that quickly fades into the background continuum at non-zero momentum [40], to the extent that it is referred to as "incoherent" [41]. In Fermi liquid theory, the plasmon is infinitely long lived at zero momentum, and only acquires a damping at momenta high enough to allow for a decay into particle-hole pairs [1]. The plasmon of holographic models, on the other hand, is damped throughout momentum space [42]. This is due to the dissipative

[3]Not to be confused with the *Planck* time $t_P = \sqrt{\hbar G/c^5} \approx 10^{-44}\,\mathrm{s}$ obtained from the units $\hbar = c = G = 1$.

mechanisms of a black hole in the gravitational theory, and can be interpreted in terms of a quantum critical sector in the strongly correlated theory [43]. The qualitative agreement motivates further research to formulate a realistic prediction of the data, which is currently being pursued [44].

Various aspects of plasmons within holographic duality have been explored, such as the effects of momentum relaxation [45], the layered nature of cuprate HTS [46], or different gravitational backgrounds [43, 47]. However, experiments using M-EELS, which inherently is a surface probe, also couple to *surface plasmons* [41, 48]. These have so far been unexplored in a holographic setting, and are the topic of paper III and Chapter 3. We show how to set the boundary conditions in the gravitational theory to be able to describe electromagnetic scattering experiments on a strange metal, and use this to extract the surface response.

Chapter 2

Kinetic Theory of Electrons

In this chapter, we cover the mathematical preliminaries and selected results of papers I and II. In Section 2.1, we discuss the kinetic equation that describes the relaxation of the weakly perturbed quasielectron distribution toward local equilibrium. Section 2.2 illustrates the method presented in Paper II of solving the kinetic equation, whereas Section 2.3 is devoted to Paper I and the shear viscosity of the electron liquid.

Kinetic theory is an old subject, and there exists a host of excellent resource material that cover the topic in great detail; see, for instance, Refs. [49–52].

2.1 The Kinetic Equation

Many-body physics is notoriously hard. While we know the governing equation — the Schrödinger equation — solving it for each of the particles in a piece of material is impossible. This computational intractability can partly be remedied by taking a statistical view of the physics. We consider the quasiparticle distribution function $f(t; \boldsymbol{r}, \boldsymbol{p})$, that acts as a probability distribution function in phase space. For instance, the density of quasiparticles is given by

$$n(t; \boldsymbol{r}) = \int \frac{\mathrm{d}\boldsymbol{p}}{(2\pi)^d} f(t; \boldsymbol{r}, \boldsymbol{p}), \tag{2.1}$$

up to a spin degeneracy factor. The explicit dependence on both the position $\boldsymbol{r}$ and momentum[1] $\hbar\boldsymbol{p}$ violates the uncertainty principle, but poses no difficulty for phenomena on length- and time scales larger than those of the atomic constituents [1]. One can therefore interpret $f(t; \boldsymbol{r}, \boldsymbol{p})$ as a "mesoscopic" occupation function of the center of the quasiparticle wave packet [53].

[1] We let $\boldsymbol{p}$ denote the wave vector, so the momentum carried by a quasiparticle wave packet is $\hbar\boldsymbol{p}$.

The dynamics of the quasiparticle distribution is governed by the semiclassical kinetic equation

$$\left(\frac{\partial}{\partial t} + \boldsymbol{v}\cdot\frac{\partial}{\partial \boldsymbol{r}} - \frac{\partial U}{\partial \boldsymbol{r}}\cdot\frac{\partial}{\partial \hbar\boldsymbol{p}}\right) f(t;\boldsymbol{r},\boldsymbol{p}) = I[f(t;\boldsymbol{r},\boldsymbol{p})] \tag{2.2}$$

where $\boldsymbol{v} = \hbar\boldsymbol{p}/m^*$ is the quasiparticle velocity, m^* the effective mass, and $\boldsymbol{F} = -\partial U/\partial \boldsymbol{r}$ the force from an external potential $U(\boldsymbol{r})$. Leaving the time derivative aside, the left-hand side takes the form of a classical Poisson bracket $\{H, f\}$ between a mean-field Hamiltonian $H = \hbar^2\boldsymbol{p}^2/2m^* + U(\boldsymbol{r})$ and the distribution function, which we refer to as the *streaming term*. In the absence of a right-hand side, Eq. (2.2) assumes the form of Hamilton's equations of motion, and indeed describes a continuity equation balancing the flow of probability through the volume element $\mathrm{d}^d\boldsymbol{r}\,\mathrm{d}^d\boldsymbol{p}$ in phase space. This continuity is broken by collisions with other quasiparticles, captured in the *collision integral* $I[f(t;\boldsymbol{p},\boldsymbol{r})]$, encoding the relaxation rate of the quasiparticles. Introducing the shorthand $f_i^{(\prime)} = f(t;\boldsymbol{r},\boldsymbol{p}_i^{(\prime)})$, the collision integral reads

$$\begin{aligned} I[f(t;\boldsymbol{r},\boldsymbol{p}_1)] = -\int \frac{\mathrm{d}\boldsymbol{p}_2\,\mathrm{d}\boldsymbol{p}_1'\,\mathrm{d}\boldsymbol{p}_2'}{(2\pi)^{2d}} W(\boldsymbol{p}_1\boldsymbol{p}_2|\boldsymbol{p}_1'\boldsymbol{p}_2') \\ \times\left[f_1 f_2(1\pm f_1')(1\pm f_2') - f_1' f_2'(1\pm f_1)(1\pm f_2)\right], \end{aligned} \tag{2.3}$$

where $W(\boldsymbol{p}_1\boldsymbol{p}_2|\boldsymbol{p}_1'\boldsymbol{p}_2')$ is a matrix element describing the scattering between states of momenta $\boldsymbol{p}_1, \boldsymbol{p}_2$ and $\boldsymbol{p}_1', \boldsymbol{p}_2'$. The two terms describe the in- and out-flux of particles scattering to/from the states with momentum $\boldsymbol{p}_1$ and $\boldsymbol{p}_2$, and the upper (lower) sign corresponds to the equation describing bosonic (fermionic) quasiparticles[2].

For energy- and momentum-conserving interactions, the kinetic equation admits the general solution

$$f(t;\boldsymbol{r},\boldsymbol{p}) = \frac{1}{e^{\beta(\varepsilon(\boldsymbol{p})-\mu-\hbar\boldsymbol{p}\cdot\boldsymbol{V})}\mp 1}, \tag{2.4}$$

where $\varepsilon(\boldsymbol{p})$ is the quasiparticle dispersion, $\boldsymbol{V}(t,\boldsymbol{r})$ is a local velocity field, and in general, the chemical potential $\mu(t,\boldsymbol{r})$ and inverse temperature $\beta = 1/k_BT(t,\boldsymbol{r})$ can also be functions of space and time. By virtue of satisfying the property of *detailed balance*,

$$\frac{f_1 f_2}{(1\pm f_1)(1\pm f_2)} = \frac{f_1' f_2'}{(1\pm f_1')(1\pm f_2')}, \tag{2.5}$$

the distribution in Eq. (2.4) is annihilated by the collision integral Eq. (2.3), so the dynamics is controlled by the streaming term alone. Eq. (2.4) generalizes the Fermi-Dirac or Bose-Einstein distributions, that have a vanishing streaming term and therefore satisfy $\partial_t f = 0$.

[2]Typically, the term *collective excitations* is used to describe bosons in this context, whereas *quasiparticles* are only of fermionic nature. For ease of discussion, we here use "quasiparticle" for both.

Limitations of the Semiclassical Description

While the streaming term $\{H, f\}$ remains the same as in a purely classical description, the semiclassical label makes itself apparent from the blocking factors $(1 \pm f)$ in the collision integral, which are of quantum origin. Eq. (2.2) can therefore be seen as a classical Boltzmann equation with a select set of important quantum effects built in, namely those of the constraints on the scattering phase space. While the above formulation can seem quite phenomenological — we are starting from an equation of motion, not an action principle — a rigorous derivation of a quantum kinetic equation can be made by starting from the Keldysh effective action [54]. Here, one performs a Wigner transformation to allow for a quantum mechanical representation of phase space [55, 56]. After an approximation of having well-defined quasiparticles[3], Eq. (2.2) emerges as a lowest-order gradient expansion of the underlying quantum theory [56]. In these steps, the memory effects (i.e., where the collision integral involves an integral over time, and there is no conservation of energy due to $\delta E \delta t \geq \hbar$) of the quantum theory are erased, limiting our discussion to timescales above the saturation of the time-energy uncertainty relation.

One could ask whether the present description of a quasiparticle distribution function is limited to low temperatures, as the quasiparticle lifetime τ_{qp} decreases with increased temperature (due to an increased collision rate), and the quasiparticle concept requires $E_{\text{qp}}\tau_{\text{qp}} \gg \hbar$ [57]. As we show in paper II, the spectrum of lifetimes we compute do indeed reach their minimum values at for $T \approx T_F$ where the thermal and quantum effects become comparable, but still satisfy the aforementioned inequality. Above the Fermi temperature, the gas transitions into a non-degenerate regime, with a typical inter-particle spacing much larger than the the thermal wavelength $\lambda_T = \sqrt{2\pi\hbar^2/m^* k_B T}$. In the collision integral, the blocking factors $(1 \pm f)$ vanish, and the background solution Eq. (2.4) takes on a Maxwell-Boltzmann form. The semiclassical kinetic equation therefore reduces to the classical Boltzmann equation, effectively describing a gas of wave packets of size λ_T.

Coupled Systems

Aside from the aforementioned limitations, we have an exact description of the physics governing the gas of interacting electrons. It is however highly non-trivial to solve the non-linear integro-differential kinetic equation, made further complicated by the fact that condensed matter systems in general contain several species of quasiparticles. Each species obey their own kinetic equation, that

[3] In the so-called *quasiparticle approximation*, the spectral function $A = -2\,\mathrm{Im}\, G^R$ (G^R being the retarded Green's function) is taken as a delta function, $A \approx 2\pi\delta(\epsilon - [\varepsilon(\boldsymbol{p}) + U - \mu])$. Even for strong interactions, where the quasiparticle approximation would be poor, an analogous equation can still be derived using a semiclassical approximation [55].

couple through the collision integral as [10];

$$\partial_t f^{(i)} - \{H^{(i)}, f^{(i)}\} = I^{(i)}[\{f^{(j)}\}], \tag{2.6}$$

where $f^{(i)}$ ($H^{(i)}$) is the distribution (Hamiltonian) of the ith species of quasiparticles. For example, the electrons in a typical metal will not only collide with other electrons, but also interact with holes, phonons and impurities. Due to the increased complexity, coupled systems are often studied in the *relaxation time approximation*; $I^{(i)}[f^{(i)}, f^{(j)}] \approx -f^{(i)}/\tau_{ij}$, where the collision integral is replaced with a single relaxation time τ_{ij} capturing the interactions between species i and j. By Matthiessen's rule, the total relaxation time of species i,

$$\frac{1}{\tau^{(i)}} = \frac{1}{\tau_{ii}} + \sum_{j \neq i} \frac{1}{\tau_{ij}}, \tag{2.7}$$

receives contributions from scattering off of both the same (τ_{ii}) and different (τ_{ij}) quasiparticle species. The dynamics are however dominated by the fastest relaxing channel, so if $\tau_{ii} \ll \tau_{ij}$, an approximate description is obtained by decoupling the ith equation from the rest. For example, impurity scattering provides the dominant pathway of momentum relaxation for electrons at low temperatures[4], which is why (non-superconducting) materials have a residual zero-temperature resistivity $\rho(T = 0) \approx m^*/ne^2\tau_{\text{imp}}$. In this thesis, we focus on systems with dominant electron-electron interactions, and therefore restrict the kinetic equation to a single species of electron quasiparticles living in two dimensions.

The Linearized Kinetic Equation

In order for something interesting to happen to the system, it must be perturbed from its equilibrium in Eq. (2.4). This can be done through a temperature or velocity gradient, an external force, or a voltage (affecting the chemical potential). This shifts the distribution of quasiparticles as $f = f_0 + \delta f$, where f_0 is the background distribution in Eq. (2.4), and we parameterize

$$\delta f = f_0(1 - f_0)\chi(t; \boldsymbol{r}, \boldsymbol{p}). \tag{2.8}$$

In this way, $\chi(t; \boldsymbol{r}, \boldsymbol{p})$ can be thought of as a perturbation to the dimensionless quasiparticle energy[5]. Within linear response theory, we assert the dependence

$$\chi(t; \boldsymbol{r}, \boldsymbol{p}) = \chi(\boldsymbol{p})e^{-i\omega t + i\boldsymbol{q}\cdot\boldsymbol{r}}, \quad \beta(t, \boldsymbol{r}) = \beta + \delta\beta e^{-i\omega t + i\boldsymbol{q}\cdot\boldsymbol{r}}, \tag{2.9}$$

[4] Impurity scattering is typically independent of temperature, whereas electron-electron and electron-phonon scattering is proportional to T^2 and T^5 at low temperatures, respectively [58]. We are also neglecting the Kondo effect, which can cause a small uptick in the resistivity at the very lowest temperatures.

[5] $f_0(1 - f_0) = (-k_B T \frac{\partial f_0}{\partial \varepsilon})$, so the time- and spatial derivatives act on $\beta(\varepsilon - \mu) - \chi(\boldsymbol{p})$; see Eq. (2.12).

and so on for $\boldsymbol{F}, \boldsymbol{V}$ and μ. The streaming term, acting on the equilibrium distribution Eq. (2.4), contributes to linear order in perturbations with

$$\{H, f_0\} = \left(-\frac{\partial f_0}{\partial \varepsilon}\right)\left[\frac{\varepsilon-\mu}{T}\boldsymbol{v}\cdot\nabla T + m^*\boldsymbol{v}^T\boldsymbol{Q}\boldsymbol{v} + \boldsymbol{v}\cdot(\nabla\mu - \boldsymbol{F})\right], \tag{2.10}$$

where $Q_{ij} = \partial_{(i}V_{j)}$ is the so-called rate-of-strain tensor[6] [52], we assume $\varepsilon = \varepsilon(\boldsymbol{p})$ and take $\boldsymbol{V} = 0$ on average (or perform a Galilean transformation to make it so). Finally, by defining the collision operator

$$\mathcal{L}[\chi(t;\boldsymbol{r},\boldsymbol{p})] = -\frac{I[\delta f(t;\boldsymbol{r},\boldsymbol{p})]}{f_0(1-f_0)}, \tag{2.11}$$

we arrive at a general form of the linearized kinetic equation

$$\beta\left(\boldsymbol{v}\cdot\boldsymbol{F} - m^*\boldsymbol{v}^T\boldsymbol{Q}\boldsymbol{v}\right) + (\partial_t + \boldsymbol{v}\cdot\nabla)\left(\beta(\varepsilon-\mu) - \chi\right) = \mathcal{L}[\chi], \tag{2.12}$$

which is the equation of interest in the following sections.

2.2 Eigenmodes of the Electron-Electron Collision Integral

Before applying Eq. (2.12) to the discussion of transport properties of the electron gas in Section 2.1, we investigate the properties of the collision operator $\mathcal{L}$ itself. In the absence of external forces, and with the temperature, chemical potential and fluid velocity kept fixed, the linearized kinetic equation takes the form of an eigenvalue problem,

$$\mathcal{L}[\chi(\boldsymbol{p})] = \gamma\chi(\boldsymbol{p}), \tag{2.13}$$

where γ is the *decay* rate[7]. $\mathcal{L}$ is a positive semi-definite Hermitian operator (see paper II), so the eigenvalues γ that describe the relaxation of the electrons toward local equilibrium are real and bounded from below; $\gamma \geq 0$. The lower limit is saturated for the so-called *zero modes* ($\gamma = 0$), that correspond to the conservation of particle number, momentum and energy.

The computation of the decay rate of the electron liquid dates back to the 60s, where it was inferred from transport coefficients obtained within Fermi liquid theory in the zero-temperature limit. This gives the now well-known result $\gamma_{ee} \sim T^2$ in three dimensions [59–61]. In two dimensions, the constrained phase space leads to a logarithmic enhancement due to small angle scattering, and a decay rate $\gamma_{ee} \sim T^2 \ln T$ at low temperatures [62–65][8]. Diagrammatic approaches that determine the decay rate via the electron self-energy,

[6] $X_{(\alpha\beta)} \equiv \frac{1}{2}(X_{\alpha\beta} + X_{\beta\alpha})$.

[7] That is, a purely decaying perturbation with $\omega = -i\gamma$ and $\boldsymbol{q} = 0$.

[8] The restriction to one spatial dimension has even more radical consequences, and leads to the Tomonaga-Luttinger liquid [66].

$\gamma_{ee} \sim -\operatorname{Im}\Sigma$, as employed in Refs. [64, 65], are however limited to the fastest decay channel. This works well when the entire spectrum of decay rates generated by Eq. (2.13) is of a similar timescale, but as shown at the end of this section, this is not the case in two dimensions. Furthermore, the low Fermi temperature of two-dimensional materials also limits the viability of low-temperature expansions with $T/T_F \ll 1$. As the kinetic description in itself can be extended to arbitrary temperatures, we now turn to an outline of the mathematical methods used in papers I and II to solve Eq. (2.13). For a further discussion on the method and its numerical implementation, see Appendices C and D in paper II.

Solving the Linearized Kinetic Equation

The crucial step for turning the kinetic equation into a concrete mathematical problem is the introduction of an inner product naturally induced by the collision integral;

$$\langle \chi' | \chi \rangle = \lambda_T^2 \int \frac{\mathrm{d}^2 \boldsymbol{p}}{(2\pi)^2} \bar{\chi}'(\boldsymbol{p}) f_0(\boldsymbol{p})(1 - f_0(\boldsymbol{p}))\chi(\boldsymbol{p}). \tag{2.14}$$

Matrix elements of the linearized collision integral operator with respect to this inner product then read

$$\langle \psi | \mathcal{L} | \chi \rangle = \frac{\lambda_T^2}{4} \int \frac{\mathrm{d}\boldsymbol{p}_1 \, \mathrm{d}\boldsymbol{p}_2 \, \mathrm{d}\boldsymbol{p}_1' \, \mathrm{d}\boldsymbol{p}_2'}{(2\pi)^8} W_{121'2'} F_{121'2'} \left[\sum_i{}' \psi(\boldsymbol{p}_i) \right] \left[\sum_i{}' \chi(\boldsymbol{p}_i) \right], \tag{2.15}$$

where the scattering matrix element $W_{121'2'} = W(\boldsymbol{p}_1 \boldsymbol{p}_2 | \boldsymbol{p}_1' \boldsymbol{p}_2')$ enforces momentum and energy conservation, $F_{121'2} = f_0(\boldsymbol{p}_1) f_0(\boldsymbol{p}_2)(1 - f_0(\boldsymbol{p}_1'))(1 - f_0(\boldsymbol{p}_2'))$ is the product of Fermi factors, and $\sum_i' x_i = x_1 + x_2 - x_1' - x_2'$. We now assume that the material has a parabolic band dispersion $\varepsilon(\boldsymbol{p}) = \hbar^2 \boldsymbol{p}^2 / 2m^*$, where m^* is the effective mass. This means that the Fermi surface is a circle, so the perturbation χ may be expanded into angular harmonics as

$$\chi(\boldsymbol{p}) = \sum_m \chi(p) e^{im\theta}, \tag{2.16}$$

with θ the polar angle on the Fermi surface. Fig. 2.1 shows the first few Fermi surface deformations for constant $\chi(p)$, which can be though of as a rigid shift in the chemical potential[9]. The angular mode number m dictates the behavior of the deformations under parity: modes with m even are parity-even, whereas modes with m odd are parity-odd. Modes of different angular mode

[9] The figures in Fig. 2.1 are drawn at zero temperature (when the Fermi-Dirac distribution is a step function), or alternatively, for a constant perturbation $\chi(p)$. Momentum-dependence in $\chi(p)$ captures the softening of the Fermi surface at finite temperature, blurring the edges in the figures.

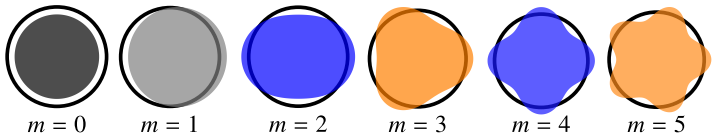

Figure 2.1: An expansion of the Fermi surface deformation $\chi(\boldsymbol{p})$ into angular harmonics labeled by a mode number m. The black circle is the Fermi energy for electrons with a parabolic dispersion $\varepsilon(\boldsymbol{p}) = \hbar^2\boldsymbol{p}^2/2m^*$.

numbers m are orthogonal with respect to the inner product, so the blocks $\mathcal{L}^{(m)} = \langle \psi e^{im\theta} | \mathcal{L} | \chi e^{im\theta} \rangle$ of the full matrix can be treated separately. In the language of Eq. (2.16), the zero modes of particle number and energy conservation live in the $m = 0$ sector and correspond to $\chi(\boldsymbol{p}) \sim 1$ and $\chi(\boldsymbol{p}) \sim p^2$, respectively, whereas the two conserved components of the total momentum are linear combinations of $\chi(p) \sim pe^{\pm i\theta}$.

The inner product allows for a basis of orthogonal polynomials $\{T_n(p)\}$ to be generated (e.g., by a Gram-Schmidt procedure), whereby the perturbations can be expanded as $\chi(p) = \sum_n^N T_n(p)$ up to an upper basis dimension N. From the collision operator matrix elements $\langle T_n | \mathcal{L}^{(m)} | T_{n'} \rangle$, one obtains a spectrum of N eigenvalues $\gamma_m^{(1)} \leq \cdots \leq \gamma_m^{(N)}$. Since $\mathcal{L}$ is a positive semi-definite Hermitian operator just like a Hamiltonian, the Rayleigh-Ritz principle guarantees that the eigenvalues converge from above as the basis dimension N is increased [67]. A lowest order, constant basis polynomial $T_1(p)$ corresponds to a rigid deformation of the Fermi surface. Higher order (momentum-dependent) polynomials incorporate the effects of finite energy transfer, and have a larger influence at higher temperatures as the broadening of the Fermi surface increases.

The numerical challenge of solving the linearized kinetic equation lies in the evaluation of the matrix elements $\langle T_n | \mathcal{L}^{(m)} | T_{n'} \rangle$, which are multidimensional integrals that at low temperatures feature highly peaked integrands due to the Fermi factors in the collision integral. To this end, the adaptive *Divonne* algorithm within the Cuba library is used, as it allows for a Monte Carlo sampling of the integrand to be biased in the peaked regions [68]. Through this mathematical formulation, a complete characterization of the eigenmode spectrum can be obtained, as was done in Ref. [69] for a constant interaction matrix element as a proof of principle. In the following subsection, we discuss a more realistic Coulomb interaction, and its ramifications on the mode spectrum.

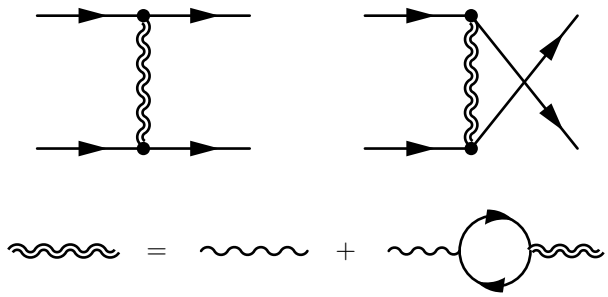

Figure 2.2: Direct and exchange-channel diagrams for the Coulomb interaction $\langle \boldsymbol{p}_1\boldsymbol{p}_2|V|\boldsymbol{p}_1'\boldsymbol{p}_2'\rangle$ (top). The RPA approximation of the Coulomb interaction is the sum over all "ring"-diagrams (bottom). In the static limit $\omega \ll qv_F$, it takes the form of the Thomas-Fermi screened interaction in Eq. (2.19).

The Screened Coulomb Interaction

The scattering element in Eq. (2.15) is within a Golden-Rule approximation given by

$$W(\boldsymbol{p}_1', \boldsymbol{p}_2'|\boldsymbol{p}_1\boldsymbol{p}_2) = \frac{2\pi}{\hbar} \left|\langle \boldsymbol{p}_1\boldsymbol{p}_2|V|\boldsymbol{p}_1'\boldsymbol{p}_2'\rangle\right|^2 (2\pi)^2 \delta\left(\sum_i{}' \boldsymbol{p}_i\right) \delta\left(\sum_i{}' \varepsilon_i\right), \quad (2.17)$$

where the delta functions ensure conservation of momentum and energy. In papers I and II, we consider a screened Coulomb interaction, acting through both direct and exchange channels[10]

$$\left|\langle \boldsymbol{p}_1\boldsymbol{p}_2|V|\boldsymbol{p}_1'\boldsymbol{p}_2'\rangle\right|^2 = \underbrace{V^2(\boldsymbol{p}_1' - \boldsymbol{p}_1) + V^2(\boldsymbol{p}_1' - \boldsymbol{p}_2)}_{\text{direct}} - \underbrace{V(\boldsymbol{p}_1' - \boldsymbol{p}_1)V(\boldsymbol{p}_1' - \boldsymbol{p}_2)}_{\text{exchange}}, \quad (2.18)$$

$$V(\boldsymbol{q}) = \frac{2\pi e^2}{q + k_{\mathrm{TF}}}, \quad (2.19)$$

where $k_{\mathrm{TF}} = 2m^*e^2/\hbar^2$ is the Thomas-Fermi wave vector. The contributing diagrams are shown in Fig. 2.2. This potential is obtained from the static ($\omega \ll qv_F$) limit of the dielectric function $\varepsilon(\omega, \boldsymbol{q})$ computed within the random phase approximation (RPA) as $V(\boldsymbol{q}) = V_0(\boldsymbol{q})/\varepsilon(\omega = 0, \boldsymbol{q})$, where $V_0(\boldsymbol{q})$ is the bare Coulomb interaction. This relates the Thomas-Fermi wave vector to the RPA density parameter r_s as $k_{\mathrm{TF}} = 2r_s\sqrt{\pi n}$, where $n = 2T_F/T\lambda_T^2$ is the density of the electron gas. The parameter r_s can be though of as the radius of the

[10]This is essentially Møller scattering, so the s-channel process is forbidden as there is no photon carrying charge $2e$.

volume containing on average one electron, where a larger value implies stronger correlations between the electrons due to the decreased screening [54]. While the RPA expansion is only strictly valid for $r_s < 1$, it empirically works well for most metals, where $r_s \sim 3 - 6$ [70].

The most pertinent critique of the choice of interaction element is the neglect of a finite energy transfer ω, that can be important at large temperatures. As is the case for the shear viscosity of the electron liquid discussed in Section 2.3, only the first few basis polynomials enter, i.e., it is primarily determined by processes with small energy transfer. Generalizing Eq. (2.19) to include the finite-temperature Lindhard function $\Pi(\omega, \boldsymbol{q}; T)$ would involve an additional integral at every point of the integrand [66], slowing down the computations. Finally, the Golden rule expression in Eq. (2.17) is a first-order Born approximation, estimating the transition T-matrix as $T \approx V$, which is valid as long as the scattering potential V is weak [71]. Higher order effects are however partly incorporated due to the RPA origin of the screened Coulomb interaction (see Fig. 2.2).

Mode Spectrum

We here present a brief synopsis of the results in paper II, which details the full spectrum of modes obtained from the eigenvalue problem in Eq. (2.13). These determine the behavior of the electron gas, impacting the transport characteristics via Eq. (2.12). Fig. 2.3(a) shows the eight lowest-lying decay rates $\gamma_m^{(n)}, n = 1, \dots 8$, for $0 \leq m \leq 20$, of the collision operator at low temperatures, $T = 0.001 T_F$. Note that the zero modes corresponding to the underlying symmetries of particle number, energy and momentum conservation — the two lowest modes for $m = 0$ and the lowest mode for $m = 1$ — have $\gamma_m = 0$ and are therefore not seen in Fig. 2.3.

By evaluating $\langle \psi^\star | \mathcal{L} | \psi^\star \rangle$ for a lowest order basis element $\psi^\star$, we are able to analytically compute $\gamma_{m=2}$ for all r_s, as is detailed in Appendix A in Paper II. This allows us to further parametrize all of the lowest-lying even modes at low temperatures as

$$\gamma_{m \text{ even}} \approx \frac{2\pi}{3\hbar} \frac{T^2}{T_F} r_s^2 \left[\log\left(1 + \frac{\sqrt{2}}{r_s}\right) - \frac{\sqrt{2}}{\sqrt{2} + r_s} \right] \frac{\ln m\phi}{\ln 2\phi} \tag{2.20}$$

for $r_s \gtrsim 1$, where the fit parameter ϕ in part absorbs the small error in using a lowest order basis polynomial. We plot Eq. (2.20) in Fig. 2.3 as a dashed gray line, where $\phi = 1.23$. Intriguingly, this gives a logarithmic scaling in the angular mode number m (up to $m \lesssim \sqrt{T_F/T}$), instead of being logarithmic in temperature as in self-energy calculations [64], that are oblivious to the symmetries of different Fermi surface deformations. On the contrary, the lowest-lying

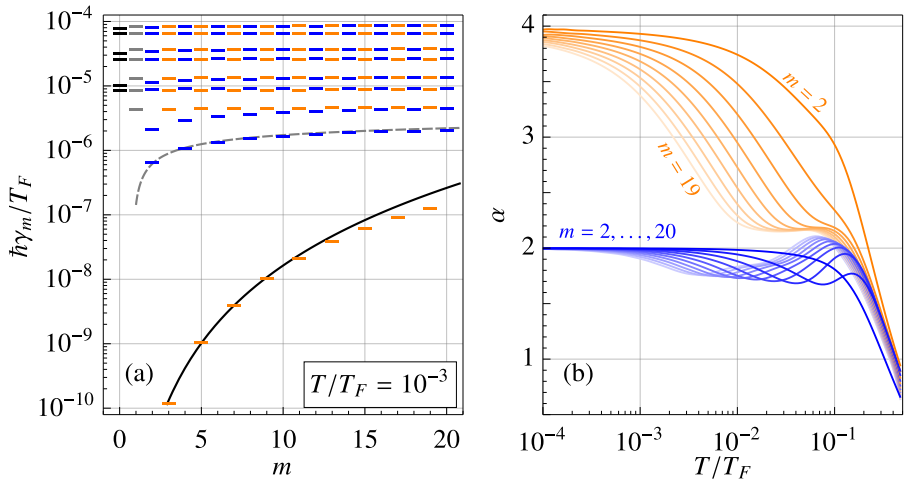

Figure 2.3: (a) Hierarchy of eigenmodes of the collision operator Eq. (2.15) at low temperature, $T = 0.001T_F$. There is a separation by several orders of magnitude between the lowest-lying parity-odd modes and the rest. The dashed gray and solid black line correspond to Eq. (2.20) and Eq. (2.21), respectively. (b) Temperature scaling exponents α for the lowest-lying modes with angular modes numbers $2 \leq m \leq 20$. Even modes are shown in blue and odd modes in orange. Lighter colors indicate higher values of m. In both figures, the interaction strength is given by $r_s = 1$.

odd modes are approximately given by

$$\gamma_{m\ \mathrm{odd}} = \frac{4\pi^3 T_F}{15\hbar} |V|^2 \left(\frac{T}{T_F}\right)^{\alpha} m^4, \tag{2.21}$$

where $|V|^2$ is the Coulomb matrix element evaluated at a small momentum transfer $q \approx 0.15k_F$ and the scaling exponent α, shown in Fig. 2.3(b), asymptotes to 4 in the low-temperature limit. As is apparent from the Fig. 2.3(a), there exists set of long-lived modes — enhanced by a factor $(T/T_F)^2$ — that correspond to parity-odd deformations of the Fermi surface. This striking separation has been dubbed the "odd-even effect" and is argued to give rise to a new transport regime in between the limits of ballistic and hydrodynamic flow [72, 73]. Here, the effective theory would be hydrodynamics, extended to to also include the long-lived, "non-hydro", odd modes. Such extensions of hydrodynamics is known as "hydro+" in the QCD community [74], or "quasihydro" within holography [75]. The regime, which has been called the "tomographic" regime [73], is predicted to harbor novel charge-neutral modes [76] and give rise to a fractional-power flow profile [73].

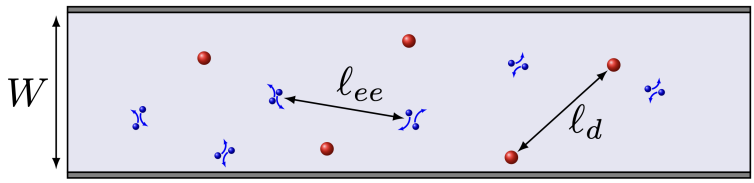

Figure 2.4: The electron fluid flowing through a channel of width W. The length scale set by electron-electron scattering (blue) is ℓ_{ee}, whereas the length scale set by scattering off impurities or disorder (red) is ℓ_d. If $\ell_{ee} \ll W \ll \ell_d$, the fluid enters a hydrodynamic regime, where the resistivity is set by the shear viscosity.

Figure 2.3(b) shows the temperature scaling exponent α for the lowest-lying even and odd modes, and highlights that the separation of long-lived, odd modes extends up to $T \approx 0.1T_F$. As shown in paper II, the magnitude of the separation is controlled by the interaction strength r_s, and can therefore be tuned in an experimental setting by chaining the doping. A complete analysis of the dependence on the interaction strength r_s, angular mode number m and temperature T/T_F is presented Paper II.

2.3 Shear Viscosity of the Electron Gas

With the ability to completely characterize the behavior of the collision operator $\mathcal{L}$, the extension to the full linearized kinetic equation in Eq. (2.12) is simply that of a linear algebra problem. A host of transport coefficients are available for analysis, and here we focus on the *shear viscosity* that quantifies the diffusion of momentum, which is the topic of Paper I [77].

To appreciate the importance of the shear viscosity, consider the flow of an (electron) liquid through a channel of width W, as is illustrated in Fig. 2.4. Electron-electron scattering sets a momentum-conserving length scale $\ell_{ee} = v\tau_{ee}$, whereas impurity or disorder scattering sets a momentum-relaxing length scale ℓ_d. When $\ell_d \ll \ell_{ee} \ll W$, the finite size of the channel plays no role, and the fluid is in a ballistic regime. Here, one can imagine the electrons as pinballs in a pinball machine hitting against bumpers (the impurities) that relaxes the momentum of the electrons. The resistivity, related to the momentum dissipation of the charge-carrying electrons, is therefore governed by the rate of impurity scattering.

On the other hand, if $\ell_{ee} \ll W \ll \ell_d$, hydrodynamic flow is achieved as the momentum-conserving electron-electron interactions allow the electrons to reach local equilibrium. Here, momentum is conserved everywhere except at the boundaries, which causes a parabolic flow profile. The fluid effectively

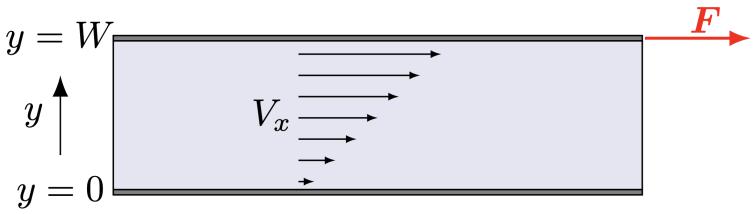

Figure 2.5: A fluid (blue) between two plates (gray) experiencing shear stress. By applying a force $\boldsymbol{F}$ to the upper plate, the fluid develops a velocity gradient $V_x(y)$. The shear viscosity is the proportionality constant between the force (per unit area) and the gradient of the fluid velocity, effectively determining the rate of momentum loss. Image adapted from [49].

flows around the impurities, and the electric resistivity is instead determined by strength of the coupling to the boundary, where momentum is lost. The extent of this momentum relaxation is quantified by the shear viscosity — a property of the electron fluid itself, and not the medium through which it flows. The stronger the interactions between the particles, the lower the resistance, as an even smaller ℓ_{ee} means that the electrons do not "find" the edges as easily.

Shear Viscosity from the Kinetic Equation

To determine the shear response, consider the *gedankenexperiment* of applying a force along one of the edges of the channel through which the fluid flows [49]. This causes a spatially varying velocity profile perpendicular to the direction of the force, as illustrated in Fig. 2.5. This gradient is captured mathematically by non-vanishing stress tensor $\sigma_{ij} = -nm^* \langle v_i v_j \rangle$, which can be decomposed into a symmetric traceless matrix and a trace,

$$\sigma_{ij} = \eta \left(\frac{\partial V_i}{\partial x_j} + \frac{\partial V_j}{\partial x_i} - \frac{2}{d} \nabla \cdot \boldsymbol{V} \delta_{ij} \right) + (\zeta \nabla \cdot \boldsymbol{V} - P)\delta_{ij}. \tag{2.22}$$

Here, d is the number of spatial dimensions, P is the pressure, and the coefficients η and ζ are the shear and bulk viscosities, respectively. By perturbing the system within linear response with a wave vector perpendicular to the fluid velocity ($\nabla \cdot \boldsymbol{V} = 0$), the shear viscosity is obtained as the proportionality coefficient between the tensors $\sigma_{ij} = 2\eta Q_{ij}$. Explicitly,

$$\eta = -\frac{nm^*}{2Q_{xy}} \langle v_x v_y \rangle = -\frac{m^*}{2Q_{xy}} \int \frac{\mathrm{d}^2 \boldsymbol{p}}{(2\pi)^2} v_x v_y \delta f(\boldsymbol{p}), \tag{2.23}$$

which involves an inversion of Eq. (2.12) to solve for $\delta f(\boldsymbol{p})$. Expressed in the basis $\{|nm\rangle = |T_n e^{im\theta}\rangle\}$ generated by the inner product Eq. (2.14), the dimen-

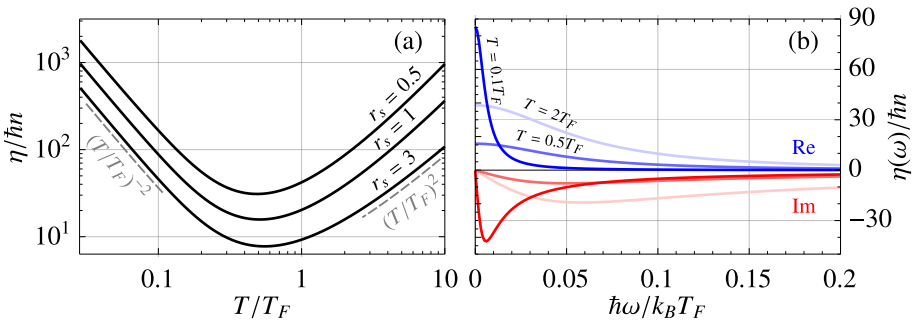

Figure 2.6: (a) Static shear viscosity for three different interaction strengths, $r_s = 0.5, 1$ and 3. The shear viscosity attains a minimum at temperatures near the Fermi temperature T_F. (b) Frequency dependent shear viscosity at three different temperatures for $r_s = 1$. The real parts are shown in red and the imaginary parts in blue. Lighter colors indicate a higher temperature.

sionless shear viscosity is obtained as

$$\frac{\eta}{\hbar n} = \frac{T}{T_F}\langle v_x v_y|(\mathcal{L} - i\omega + i\boldsymbol{v}\cdot\boldsymbol{q})^{-1}|v_x v_y\rangle. \tag{2.24}$$

Due to the orthogonality of angular harmonics,

$$|v_x v_y\rangle = \frac{\lambda_T^2}{2}\int \frac{\mathrm{d}\boldsymbol{p}}{(2\pi)^2} v^2 \sin 2\theta \chi(p) e^{im\theta} \sim \delta_{m,2}, \tag{2.25}$$

which means that $\eta(\omega, \boldsymbol{q} = 0)$ is entirely determined by dynamics of the quadrupole $m = 2$ mode[11].

In Fig. 2.6(a), we plot the static shear viscosity at three different interaction strengths, $r_s = 0.5, 1$ and 3. It is related to the shear relaxation time τ_η as $\eta = P\tau_\eta$, which means that $\tau_\eta \approx \tau_{m=2}$, and not τ_{ee} as obtained by e.g., self-energy calculations. The pressure asymptotes to the constant value $P = nE_F/2$ at low temperatures and the ideal gas pressure $P = (T/T_F)nE_F$ at high temperatures, which together with

$$\begin{cases} \tau_{m=2} & \sim (T_F/T)^2, \quad T \ll T_F, \\ \tau_{m=2} & \sim (T_F/T)^{-1}, \quad T \gg T_F, \end{cases} \tag{2.26}$$

leads to a diverging shear viscosity at both low and high temperatures. In particular, the viscosity attains a minimum at intermediate temperatures, which

[11] The term $i\boldsymbol{v}\cdot\boldsymbol{q}$ is not a diagonal matrix in m-space, which implies a coupling to modes of other m at finite $\boldsymbol{q}$.

is of particular interest as the famous Kovtun-Son-Starinets (KSS) bound (obtained from holography — see Chapter 3) postulates that $\eta/s \geq \hbar/4\pi$, where s is the entropy density. For the non-relativistic case at hand, a saturation of this bound would imply $E_F \ll \hbar\gamma$, invalidating the quasiparticle description. The electron liquid would then enter a regime with such strong correlations that it is more aptly described by the methods presented in Chapter 3. For the two-dimensional electron liquid interacting through a screened Coulomb interaction discussed here, we find that the minimum is larger than the KSS bound by at least a factor of 50, and the quasiparticle description remains valid.

At finite frequency, the shear viscosity can be expressed as a complex-valued function, $\tilde{\eta}(\omega) = \eta(\omega) - i\omega\tau_\eta\eta(\omega)$, where $\eta(\omega)$ assumes the form

$$\eta(\omega) = \frac{P\tau_\eta}{1 + (\omega\tau_\eta)^2}. \tag{2.27}$$

The pressure of the non-interacting electron gas is given by

$$P = -n\varepsilon_F \left(\frac{T}{T_F}\right)^2 \mathrm{Li}_2(-e^{\beta\mu}) \tag{2.28}$$

where Li_2 is the polylogarithm. The real and imaginary parts of the complex shear viscosity $\tilde{\eta}(\omega)$ is shown in Fig. 2.6(b) for three different temperatures with the interaction strength $r_s = 1$. At low temperatures, the shear viscosity diverges at small frequencies, signaling that the system behaves hydodynamically only for $\omega \to 0$. For temperatures near T_F, on the other hand, there is a significant broadening of the response function. This highlights that the hydrodynamic behavior $\eta \sim P\tau_\eta$, that holds for $\omega\tau_\eta \ll 1$, extends up to a sizeable fraction of the Fermi energy. This is the hydrodynamic regime, as depicted in Fig. 1.1, enabled by the strong electron-electron correlations near T_F.

This ends the discussion of kinetic theory and hydrodynamics, and in the next chapter, we move on to systems with even stronger correlations, where the quasiparticle picture fails.

Chapter 3

Holographic Models of Collective Charge Oscillations

In this chapter, we leave the realm of quasiparticle-based descriptions of transport in metals, and turn to the holographic duality and how it can be used to probe the physics of strongly correlated condensed matter systems. We focus on the description of collective charge oscillations known as plasmons, and in particular, surface plasmon polaritons, which is the topic of paper III.

A detailed discussion on the use of holographic methods in strongly correlated systems can be found in the large body of introductory literature, for example, Refs. [37, 78–80]. This chapter uses natural units, where $c = \hbar = k_B = 1$.

3.1 The Holographic Duality

At its core, holography is a duality between a quantum field theory (QFT), and a gravitational theory living in a higher dimension. Originally, the duality started out as the "AdS/CFT correspondence", in arguably the most influential paper in theoretical physics in the last 30 years [81]. In Maldacena's original formulation, he argued that $\mathcal{N} = 4$ Super Yang-Mills theory admits a dual description as supergravity on $\mathrm{AdS}_5 \times S^5$. In the limit of infinite 't Hooft coupling λN^2 in the gauge theory, where λ is the coupling constant and N is the rank of the gauge group, the duality reduces to that between a conformal quantum field theory (CFT) and a classical gravity theory [79]. The latter should describe a spacetime that asymptotes to anti-de Sitter (AdS) space, a solution to Einstein's equations with a negative cosmological constant.

AdS space exhibits the peculiar property that light-like paths reach spatial infinity in a finite time, and accordingly, the boundary of the space plays an important role. While AdS is the Lorentzian equivalent of a hyperbolic manifold, we can imagine a spherical volume, where the boundary is at a radius that

corresponds to the radial AdS coordinate being at infinity. One then interprets the dual CFT as living on the lower-dimensional boundary, whereas the gravity theory in AdS is said to be in "the bulk". The extra dimension can intuitively be though of as an energy coordinate, where the asymptotic AdS at radial infinity describes the high-energy (UV) content of the boundary theory, whereas the low-energy (IR) physics is controlled by the physics in the deep interior of the bulk. Refinements of the duality showed that the boundary theory only needs to be conformal at high energies, where a finite temperature black hole in the bulk breaks the scale invariance at lower energies. This means that black holes — that relax on a Planckian timescale — determines the IR behavior of the dual theory, which is one attractive feature of using the duality to describe strange metal physics, as hinted at in the introduction.

The emergence of more general dualities led the framework to become known also as "gauge/gravity duality", dropping the explicit reference to conformal symmetries [78]. This is not a perfect label either, as one can obtain gravity on the boundary as well [82, 83]. We therefore designate the machinery as simply 'the holographic duality', referring to how D-dimensional information can be completely encapsulated in a $(D-1)$–dimensional object, like in a hologram. Today, holographic theories can capture many of the essential features of condensed matter systems, such as compressible matter at finite density [79], breaking of translational symmetry [84, 85], Fermi surfaces [86–88], and long-range Coulomb interactions [42, 43, 46, 89].

In the original AdS/CFT formulation, the duality was formulated from a so-called top-down perspective, where one starts from a theory of quantum gravity and reduces it to a classical action. However, as the emergent infrared physics we are concerned with does not depend on the ultraviolet details, one can equally well start from a reasonable bulk action that includes the essential elements we are interested in. This is called a "bottom-up" approach and is the one we use in this thesis. Many of the most used holographic bottom-up models do in fact appear from consistent truncations of a full string theory.

The duality is made concrete in terms of a *holographic dictionary* that maps objects in the boundary theory to ones in the bulk. This can be made quite long depending on the content of the theory, so we focus in the following on the key entries relevant for this thesis.

The Dictionary

The boundary quantum field theory is described by the partition function

$$Z_{\mathrm{QFT}}[h(x)] \equiv \int \mathcal{D}\Phi \, e^{i \int \mathrm{d}^{d+1}x \, [\mathcal{L} + h(x)\mathcal{O}(x)]}, \tag{3.1}$$

where Φ denotes all degrees of freedom in the theory and $\mathcal{L}$ is the Lagrangian. The partition function acts as a generating functional via the inclusion of the

source $h(x)$ to the operator $\mathcal{O}(x)$, so that n-point functions $\langle \mathcal{O}\mathcal{O}\ldots\rangle$ are obtained through successive functional derivatives of the partition function with respect to $h(x)$. The essence of the holographic duality is captured in the Gubser-Klebanov-Polyakov-Witten (GKPW) formula [90, 91], which is the equality between the partition functions

$$Z_{\mathrm{QFT}}[h(x)] = Z_{\mathrm{Grav}}[h(x)], \tag{3.2}$$

where Z_{Grav} is the partition function of the bulk gravitational theory,

$$Z_{\mathrm{Grav}}[h(x)] \equiv \int^{\phi\to h} \mathcal{D}\phi\, e^{iS_{\mathrm{Grav}}[\phi]} \approx e^{iS_{\mathrm{Grav}}[\phi^*]} \tag{3.3}$$

where ϕ denotes the degrees of freedom in the bulk theory. In the limit of large 't Hooft coupling λN^2 in the field theory, stringy gravity in the bulk reduces to classical gravity [79]. This corresponds to the saddle point approximation of the partition function, where the path integral is evaluated on the solutions to the bulk equations of motion, ϕ^*, as indicated in Eq. (3.3). On this side of the duality, $h(x)$ is the value of the bulk field ϕ dual to the operator $\mathcal{O}$ at the boundary of AdS space, here schematically represented as $\phi \to h$. The dictionary entries relevant for this thesis[1] are that a bulk $U(1)$ gauge field A_μ corresponds to a conserved $U(1)$ current $\mathcal{J}^\mu$ on the boundary (a topic which we will return to in Section 3.2), and the bulk metric $g_{\mu\nu}$ is dual to the boundary stress-energy tensor $\mathcal{T}^{\mu\nu}$.

When combined with the saddle point approximation in the bulk, the GKPW formula Eq. (3.2) imply that n-point functions in the boundary theory to be obtained in terms of the solutions to the bulk equations of motion as

$$\langle \mathcal{O}(x_1)\ldots\mathcal{O}(x_n)\rangle = \frac{\delta^n S_{\mathrm{Grav}}[\phi^*]}{\delta h(x_1)\ldots\delta h(x_n)}, \tag{3.4}$$

where the solutions ϕ^* are subject to the boundary conditions $\lim_{r\to\infty}\phi(x,r) = h(x)$. The problem of computing n-point functions in the strongly coupled field theory has therefore been reduced to that of solving Einstein's equations in the dual bulk theory.

We saw in Section 2.3 that the stress tensor encodes the shear viscosity. By using Eq. (3.4), Kovtun, Son, and Starinets obtained the shear viscosity in a holographic theory from the two-point function $\langle \mathcal{T}_{xy}\mathcal{T}_{xy}\rangle$, which led them to conjecture the lower bound $\eta/s \geq \hbar/4\pi$ [92]. The bound is saturated for any theory with a gravity dual — that is, for a boundary theory with correlations strong enough that the bulk is described purely by classical gravity, as in Eq. (3.3). Such a minimum viscosity is a telltale sign of strongly correlated

[1] It is in general not trivial to identify which field corresponds to what operator, but they must share symmetry properties, which greatly restricts the number of possible options.

physics, and has been observed in the quark-gluon plasma created by colliding nuclei at high energies [93]. We saw in Fig. 2.5 that the shear viscosity reached its minimum near T_F, where the electron-electron interactions became dominant enough for the electron fluid to enter a hydrodynamic regime. One could then ask if the strange metal, with its absence of quasiparticles and arguably even stronger correlations, is also described by hydrodynamics. Experimental evidence of hydrodynamic behavior in strange metals, such as a turbulent electron flow, would be a smoking gun for holography providing the proper framework for understanding these materials.

The Reissner-Nordström Background

The workhorse for most holographic applications to condensed matter problems is the *Reissner-Nordström* (RN) model, being the simplest black hole solution that is able to capture electromagnetic phenomena. It is obtained from the Einstein-Maxwell bulk action

$$S_{EM} = \frac{1}{2\kappa^2}\int \mathrm{d}^{d+2}x\sqrt{-g}\,(R-2\Lambda) - \frac{1}{4g_F^2}\int \mathrm{d}^{d+2}x\sqrt{-g}\,F_{\mu\nu}F^{\mu\nu}, \tag{3.5}$$

where d denotes the number of spatial dimensions in the boundary theory, $\kappa^2 = 8\pi G$ is Einstein's gravitational constant, g_F the coupling constant of the bulk $U(1)$ gauge field and $\Lambda = -d(d+1)/2L^2$ is the negative cosmological constant needed to make spacetime asymptotically AdS. The theory admits charged black hole background solutions of the form

$$\mathrm{d}s^2 = \frac{L^2}{\zeta^2}\left(-f(\zeta)\,\mathrm{d}t^2 + \mathrm{d}x_i^2 + \frac{1}{f(\zeta)}\,\mathrm{d}\zeta^2\right). \tag{3.6}$$

Here, the metric is expressed in Poincaré coordinates, where $\zeta = L^2/r$ is an inverted radial coordinate, such that the boundary at spatial infinity is located at $\zeta = 0$. For the gauge field, we consider solutions of the form $A = a(\zeta)\,\mathrm{d}t$, whereby the emblackening factor and background gauge potential can be expressed as

$$f(\zeta) = 1 - M\zeta^{d+1} + Q^2\zeta^{2d}, \quad a(\zeta) = \mu(1-\zeta^{d-1}), \tag{3.7}$$

where μ is the chemical potential of the boundary theory[2], we have set $L = 1$, and without loss of generality fixed the black hole horizon at $\zeta_h = 1$. The black hole has a mass M and charge Q related to the chemical potential as

$$M = 1 + Q^2, \quad Q = \sqrt{\frac{d}{2(d-1)}}\frac{\kappa}{g_F}\mu, \tag{3.8}$$

[2]This follows from the holographic dictionary; with the boundary and bulk gauge fields identified across the boundary, $A_t(\zeta \to 0) = \mathcal{A}_t$, we get $\mathcal{A}_t\mathcal{J}^t = \mu\rho$, where ρ is the density.

and a (Hawking) temperature and entropy density [37]

$$T = \frac{1}{4\pi}\left(1 + d - \frac{d\kappa^2\mu^2}{2g_F^2}\right), \quad s = \frac{2\pi}{\kappa^2}. \tag{3.9}$$

According to the holographic dictionary, this is also the temperature and entropy density of the boundary theory. The characteristics of the model is controlled by the dimensionless ratio μ/T. At $\mu/T = 0$, the black hole is charge neutral, and the boundary theory is at zero density; as $\mu/T \to \infty$, one describes an extremal black hole whose mass is entirely given by its charge and a theory at zero temperature. Crucially, a non-zero value of μ/T provides a dual field theory at finite density, and is therefore the backbone of most holographic models of condensed matter systems [37].

The RN model is somewhat pathological, as indicated by the non-vanishing ground state entropy s as $T \to 0$. This can be remedied by studying more complicated Einstein-Maxwell-Dilaton (EMD) models that feature an additional scalar field. The background geometry is then characterized by the dynamical critical and hyperscaling-violating exponents z and θ, and has a ground state entropy density $s \sim T^{(d-\theta)/z}$. This allows theories with $z \to \infty$, $\theta \to -\infty$ with z/θ fixed to achieve an entropy with and expected temperature dependence [79]. The effect of such geometries on the plasmon response was studied in Ref. [43]. While the lineshape is slightly affected, the general conclusions at the level of qualitative statements do not change. For simplicity, we stick to the RN model, knowing that it can easily be extended at any point in order to fix the thermodynamics of the boundary theory.

Finally, there is a choice to be made between two and three spatial dimensions d for the boundary theory, which on the bulk side means either AdS_4 or AdS_5. Most often, the simpler AdS_4 suffices, or is more relevant (for instance, most of the conduction in cuprate high-temperature superconductors happens along the copper oxide planes). In Section 3.3, we want to study phenomena that require the full, dynamic Maxwell equations in three dimensions, and therefore proceed with AdS_5.

Linearized Equations of Motion

To compute n-point correlators of the boundary theory, we use the Green-Kubo formalism, treating the system within linear response. Perturbing the bulk fields as $g_{\mu\nu} \to g_{\mu\nu} + \delta g_{\mu\nu}$, $A_\mu \to A_\mu + \delta A_\mu$ around the background in Eq. (3.6), gives the linearized Einstein and Maxwell equations

$$\delta G_{\mu\nu} + \Lambda \delta g_{\mu\nu} = \kappa^2 \delta T_{\mu\nu}, \quad \nabla_\mu \delta F^{\mu\nu} = 0, \tag{3.10}$$

where the stress-energy tensor $T_{\mu\nu} = -g_F^{-2}(F_{\mu\rho}F^{\rho\nu} + g_{\mu\nu}F_{\rho\sigma}F^{\rho\sigma}/(d+2))$. As we saw in Eq. (3.4), the challenge of holography lies in the solving these equations. The coupled ordinary differential equations in Eq. (3.10) are not as

innocuous as they seem, as the spacetime geometry makes them singular at both the horizon and boundary, and they are plagued by the gauge invariance of the fields. This can be dealt with by tricks used in numerical relativity [94]. Instead of imposing, for instance, the de Donder and Lorenz gauge choices[3],

$$\tau_\mu = \nabla^\nu \left(\delta g_{\mu\nu} - \frac{1}{2} g_{\mu\nu} \delta g_\rho{}^\rho \right) = 0, \quad \vartheta = \nabla^\mu \delta A_\mu = 0, \tag{3.11}$$

a priori, one can instead shift the linearized equations as

$$\begin{aligned} \delta G_{\mu\nu} &\to \delta G_{\mu\nu} - \nabla_{(\mu} \tau_{\nu)}, \\ \delta(\nabla_\mu F^{\mu\nu}) &\to \delta(\nabla_\mu F^{\mu\nu}) + \nabla^\nu \vartheta. \end{aligned} \tag{3.12}$$

Referred to as the "de Turck trick" [94], this shift makes the equations elliptic and the boundary value problem well-posed [95]. Furthermore, one avoids the spurious pure gauge modes that arise from fixing a gauge at the start[4].

Finally, the singular nature of the equations can be dealt with through the use of a pseudospectral algorithm [96]. Here, the derivative operators are discretized into dense matrices on a Chebyshev-Lobatto grid,

$$\zeta_\ell = \frac{1}{2} \left(1 - \cos \left[\pi \frac{\ell - 1}{N - 1} \right] \right), \quad \ell = 1, \ldots, N, \tag{3.13}$$

and the fluctuations $\{\delta g_{\mu\mu}, \delta A_\mu\}$ are expanded in a series of (the cardinal functions of) Chebyshev polynomials. This brings the system of equations to a linear problem on the form $L_{pq}\Phi_q = 0$, where L_{pq} is the discretized differential operator and Φ_q contains the fluctuations at all gridpoints. As the grid is determined by the zeros of these polynomials, the solutions are prevented from diverging at the endpoints. The pseudospectral algorithm also exhibits exponential convergence with respect to the grid size N (compared to e.g., a Runge-Kutta algorithm, that requires tiny step sizes at the singular endpoints), and is powerful enough as to solve even $2+1$-dimensional PDEs [97, 98]. Finally, the mapping onto a matrix problem makes it easy to impose the boundary conditions by changing the rows of L_{pq} corresponding to the endpoints $\zeta = 0$ and $\zeta = 1$. For a discussion on the application of pseudospectral methods in holography, see Refs. [99, 100], and for the specific equations relevant in this thesis, see appendix A in paper III.

Boundary Green's Functions

With the linearized equations of motion solved, we now turn to the application of Eq. (3.4) in order to determine the boundary n-point functions. From the

[3] One could also use gauge-invariant variables, but while the construction such variables is not particularly difficult, re-writing the equations of motion in terms of them poses a much larger challenge.

[4] This method effectively gives the pure gauge modes a kinetic term, putting them on the same footing as the physical modes.

viewpoint of linear response theory, the boundary operator $\mathcal{O}$ in the generating functional is the response to the source h, which in the case at hand is to be interpreted as the boundary values for the bulk fields A_μ and $g_{\mu\nu}$. As an example, we consider here the Maxwell part of the bulk action. From the equations of motion, one infers that the near-boundary expansion of the gauge-field[5] is

$$A_\mu = a_\mu^{(0)} + a_\mu^{(1)} \zeta^{d-1} + \ldots, \tag{3.14}$$

where $a_\mu^{(0)}$ and $a_\mu^{(1)}$ are the integration constants of the two linearly independent solutions to the bulk equations on motion, that need to be fixed by boundary conditions. The first one, $a_\mu^{(0)}$, is fixed by the boundary condition "$\phi \to h$". The gauge field A_μ in the bulk is dual to the current operator $\mathcal{J}^\mu$ on the boundary, whose source is a boundary gauge field $\mathcal{A}_\mu$, and is thus identified with $a_\mu^{(0)}$, the boundary value of A_μ. The second one, $a_\mu^{(1)}$, becomes related to the first by demanding infalling boundary conditions[6] at the black hole horizon. This is the key in the computation of the boundary correlation functions: it is effectively the black hole that sets the relation between the source and the response, thus determining all of the n-point functions $\langle \mathcal{O}\mathcal{O}\ldots \rangle$ on the boundary. Infalling boundary conditions respect causality in the bulk, which indeed is also the case on the boundary, where one obtains the retarded Green's function $G_R(x-y)$[7].

Equation (3.4) now necessitates the evaluation of the on-shell action. Upon partial integration, the bulk term containing the equations of motion vanishes, leaving a boundary term at spatial infinity,

$$S^* = -\frac{1}{2} \oint_{\partial \mathrm{AdS}} \sqrt{-\gamma}\, \mathrm{d}^{d+1}x\, A_\mu n_\nu F^{\nu\mu}, \tag{3.15}$$

where $\gamma_{\mu\nu}$ is the induced boundary metric and n_ν is an outward pointing unit normal on the boundary; $n_\mu n_\nu g^{\mu\nu} = 1$. Using the near-boundary expansion in Eq. (3.14), the integrand can be re-written as $a_\mu^{(0)} \eta^{\mu\nu} a_\nu^{(1)}$, where the sub-leading component is picked up by the radial derivative in $n_\zeta F^{\zeta\mu}$. The variational derivative of the on-shell action in Eq. (3.15) with respect to the source $\mathcal{A}_\mu = a_\mu^{(0)}$ then leads to the identification $\langle \mathcal{J}^\mu \rangle = (d-1)\eta^{\mu\nu} a_\nu^{(1)}$ of the boundary current in terms of the sub-leading component of the near-boundary expansion. If we for simplicity take the response to only depend on relative time and spatial coordinates, the source-response relation can be written as $\mathcal{J}^\mu(\omega, \boldsymbol{k}) = \Pi^{\mu\nu}(\omega, \boldsymbol{k}) \mathcal{A}_\nu(\omega, \boldsymbol{k})$ in Fourier space. The application of Eq. (3.4)

[5] We here disregard terms $\sim \zeta^2 \ln \zeta$ that appear in AdS_5. These are renormalized away anyway (see paper III), and would thus unnecessarily complicate the current discussion.

[6] These are automatically imposed by switching to infalling Eddington-Finkelstein coordinates with a new time coordinate v related to the old as $\mathrm{d}v = \mathrm{d}t - \mathrm{d}\zeta / f(\zeta)$.

[7] Outgoing boundary conditions at the black hole horizon would instead give the advanced Green's function on the boundary.

then implies that the Green's function $\Pi^{\mu\nu}(\omega, \boldsymbol{k})$ is obtained by two variational derivatives with respect to the source, which gives $\Pi_{\mu\nu} \sim a_\mu^{(1)}/a_\nu^{(0)}$.

From this approach to holography, one only obtains the source-operator term $\mathcal{A}_\mu \mathcal{J}^\mu$, so the boundary gauge field $\mathcal{A}_\mu$ is not *dynamical*. By performing a gauge transformation $A_\mu \to A_\mu + \nabla_\mu \theta$ in Eq. (3.15) and partially integrating, one concludes that $\nabla_\mu \mathcal{J}^\mu = 0$ in order for the boundary theory to be invariant under gauge transformations in the bulk. The boundary current is therefore the conserved current under a global $U(1)$. Much of the early work in holography was done in this way, which means that seminal papers on holographic superconductors [101] did in fact not describe superconductors, which posses a local $U(1)$ symmetry, but rather superfluids [102]. Only recently has a proper model of a holographic superconductor appeared [103], that imposes so-called dynamical boundary conditions that make the boundary theory contain a $U(1)$ gauge theory. These boundary conditions, and the phenomena they give rise to, are the topic of the next section.

3.2 Dynamical Boundary Conditions

In the above, we have described how the current responds to an external gauge field. This is perfectly fine if one wishes to compute the conductivity $\sigma(\omega, \boldsymbol{k}) = \Pi^{xx}(\omega, \boldsymbol{k})/i\omega$, but it does not correspond to dynamical electromagnetism in the boundary theory. For that to be the case, the boundary gauge field $\mathcal{A}_\mu$ should evolve according to Maxwell's equations. In this section, we discuss how to adjust the boundary conditions in the Maxwell sector of a holographic theory to achieve precisely this. Modified boundary conditions has been used to study the collective excitations known as *plasmons* [42–47, 104–107], magnetohydrodynamics [108, 109], and even dynamical gravity in the boundary theory [83].

In the process of doing linear response, we can view the boundary action as being perturbed as $S = S_0 + \delta S[\mathcal{A}_\mu]$, where the latter is the source-response term we obtained in Eq. (3.15). S_0 is the action of the strongly correlated theory, which exhibits some complicated dependence on $\mathcal{A}_\mu$ that we do not know about. To implement dynamical electromagnetism on the boundary, we assert that the boundary action also contains the term

$$S_{\text{EM}} = \int \mathrm{d}^{d+1}x \left(-\frac{1}{4e^2} \mathcal{F}_{\mu\nu}\mathcal{F}^{\mu\nu} + \mathcal{J}^\mu \mathcal{A}_\mu \right), \tag{3.16}$$

where $\mathcal{F} = \mathrm{d}\mathcal{A}$. By integrating out the gauge field, one obtains

$$S_{\text{EM}} = \frac{e^2}{2} \int \mathrm{d}^{d+1}x \, \mathcal{J}^\mu \mathcal{V}_{\mu\nu} \mathcal{J}^\nu, \tag{3.17}$$

where the photon propagator $\mathcal{V}_{\mu\nu} = [\eta_{\mu\nu}k^2 - (1-\xi)k_\mu k_\nu]/k^4$ in momentum space, k_μ is the 4-momentum, and ξ is a gauge fixing parameter [110]. Adding an expression of this type as a boundary term in the holographic theory is known as a double-trace deformation[8] and does not modify the bulk equations of motion. Following the identification of the radial coordinate as the energy scale, such a procedure can be interpreted as a relevant UV deformation that induces a flow towards a new IR fix point [37]. This keeps the identification of the operator $\mathcal{J}^\mu$ in terms of the subleading component in the near-boundary expansion the same, but changes the two-point function and the boundary conditions for the dual bulk field.

By still identifying the boundary gauge field $\mathcal{A}_\mu$ with the leading coefficient $a_\mu^{(0)}$ as before, the modified boundary action can be written as

$$S^* = \frac{1}{2}\int \mathrm{d}^{d+1}x \left(\mathcal{A}_\mu + e^2\mathcal{V}_{\mu\nu}\mathcal{J}^\nu\right)\mathcal{J}^\mu. \tag{3.18}$$

Thus, while the near-boundary expansion is the same as before — the bulk equations of motion has not changed — the source term is now given by $s_\mu = a_\mu^{(0)} + e^2\mathcal{V}_{\mu\nu}\mathcal{J}^\nu$. Linear response theory now says that $\mathcal{J}^\mu = \chi^{\mu\nu}s_\nu$, where $\chi^{\mu\nu}$ is the Green's function in the presence of the modified boundary conditions. Since both the current and boundary gauge field are unchanged, $\mathcal{J}^\mu = \Pi^{\mu\nu}\mathcal{A}_\nu$ still holds, and by equating the two expressions, we find that

$$\chi^{\mu\nu} = \left(\delta^\sigma_\nu + e^2\Pi^{\rho\sigma}\mathcal{V}_{\nu\rho}\right)^{-1}\Pi^{\mu\sigma}. \tag{3.19}$$

In particular, the density-density response function becomes

$$\langle\rho\rho\rangle = \chi^{tt} = \frac{\Pi^{tt}}{1 - \frac{e^2}{\boldsymbol{k}^2}\Pi^{tt}}. \tag{3.20}$$

This form of the response function looks similar to that of the RPA, but note that $\Pi^{\mu\nu}$ is very different from its typical designation in condensed matter physics as the free electron Green's function. Here, it is instead the Green's function for a collective oscillation in a strongly correlated system [111].

Bulk Plasmons

In order to extract the response function $\chi_{\mu\nu} \sim a_\mu^{(1)}/s_\nu$, one fixes a component of s_μ, and sets the rest to zero, which means that the boundary conditions for the bulk gauge field are a mix of Dirichlet and Neumann; so-called Robin boundary conditions. The implications of these boundary conditions can be

[8] For a general non-Abelian gauge theory, the operator $\mathcal{O}$ (here $\mathcal{O} = \mathcal{J}^\mu$) involves a trace over the gauge group. The addition of a term $\sim \mathcal{O}^2$ is therefore a "double-trace" deformation.

understood by considering the situation when all components of the source s_μ are equal to zero. This implies that

$$\Box \mathcal{A}^\mu + \partial^\mu \partial_\nu \mathcal{A}^\nu - e^2 \mathcal{J}^\mu = 0, \tag{3.21}$$

which is nothing else than Maxwell's equations in the boundary theory. A non-zero value of s_μ implies a right-hand side to this equation, so by taking the standpoint that the deformed theory obeys Maxwell's equations, the right-hand side must be interpreted as an *external* current $\mathcal{J}^\mu_{\text{ext}}$. Eq. (3.21) then describes the evolution of the gauge field for a system with a total current $\mathcal{J}^\mu_{\text{tot}} = \mathcal{J}^\mu + \mathcal{J}^\mu_{\text{ext}}$. The process of fixing a component of s_μ for the extraction of the response function can therefore be interpreted as applying an external current to the system, where $\chi^{\mu\nu}$ details how both the dynamical gauge field $\mathcal{A}_\mu$ and the internal current $\mathcal{J}^\mu$ responds.

Non-trivial solutions to Eq. (3.21) in the absence of an external current are either photons, for which the current $\mathcal{J}^\mu$ is zero, or plasmons. The latter are longitudinally polarized, collective modes that can appear when the electromagnetic wave travels through a polarizable medium[9]. Plasmons are formed by fluctuations in the charge density of a material, which causes a non-zero electric field given by the polarization. In order to distinguish them from other types of plasmons we will discuss later, we refer to these as *bulk* plasmons.

The bulk plasmon, in its nature as a self-sustained excitation, shows up as a pole in the response function $\chi^{\mu\nu}$. Figure 3.1(a) shows the imaginary part of the density-density response function χ^{tt} computed within the holographic model at $T = 0.02\mu$. The exact bulk plasmon dispersion, shown in panel (b), is obtained by solving a secular equation, i.e., finding the $\omega(\boldsymbol{k})$ for which there exists a non-trivial solution when all sources are set to zero. Both panels highlight the existence of a gapped mode, dispersing quadtratically with the momentum. This is similar to the plasmon in condensed matter textbooks [1, 66], but it differs greatly in the imaginary part, where there is finite damping even at zero momentum [42]. Typically, a finite linewidth is only achieved at momenta high enough to allow a decay into particle-hole pairs: the so-called Lindhard continuum. Here, the decay has been argued to be due a "quantum critical continuum" instead [43].

The plasmons response in strange metals have been investigated experimentally using both optics [112] and M-EELS [40, 113], which show a plasmon at $\boldsymbol{k} = 0$ that is overdamped[10]. While experimental agreement should not be expected for such a simple model as the one presented here, where effects such

[9]The fact that $\mathcal{A}_\mu$ has gained an extra degree of freedom, as if it were massive, can be interpreted as the Goldstone boson of the spontaneously broken Galilean symmetry being eaten by the photon.

[10]A reconciliation of the different data created some argument [114, 115], but appears to have been settled [41]. The consensus seems to be that the there exists a broad, "incoherent", plasmon near $\boldsymbol{k} = 0$, that decays very rapidly at larger momenta.

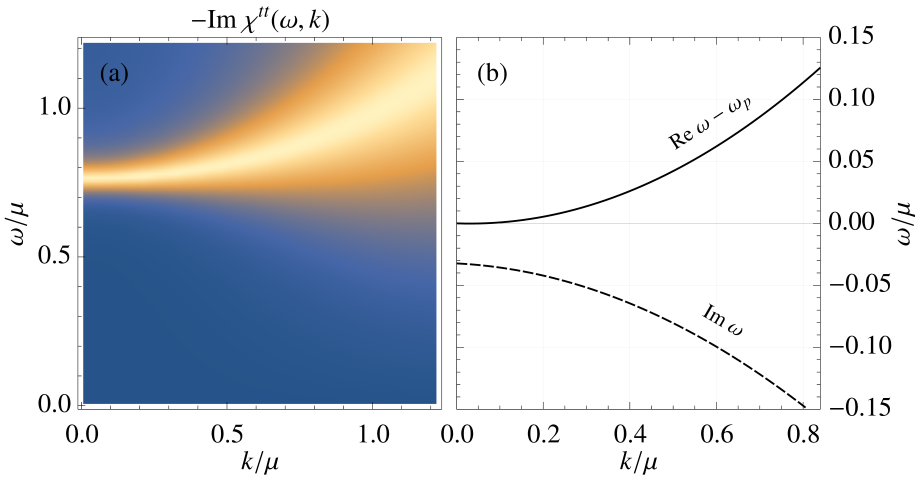

Figure 3.1: (a) Imaginary part of the density-density correlator $-\operatorname{Im}\chi^{tt}(\omega, \boldsymbol{k})$ obtained in a holographic RN model with modified boundary conditions at a temperature $T = 0.02\mu$. The function has been normalized to its peak value for each value of $\boldsymbol{k}$ for visibility, and lighter colors indicate a larger value. (b) Exact dispersion $\omega^*(\boldsymbol{k})$ of the holographic bulk plasmon. The real part has the plasma frequency $\omega_p = \omega^*(\boldsymbol{k} = 0)$ subtracted for clarity. The imaginary part shows the significant damping of the plasmon even at $\boldsymbol{k} = 0$.

as those of the lattice or the layered nature of the materials clearly is missing, it is remarkable how the dynamics of the black hole provides a mechanism that allows for a large damping even at zero momentum. A simple idea for a layered model was proposed in [46], which shows an acoustic plasmon mode similar to those seen in experiments using angle-resolved photon emission spectroscopy [116], that also are of an incoherent nature.

Out of the experimental techniques that can probe the plasmon response, it is arguably M-EELS that provides the most information, as it measures it throughout frequency and momentum space at meV precision [117]. However, M-EELS is inherently a surface probe, and measures both the surface and bulk response of the material [48]. A complete description of strange metal plasmons using holographic models therefore requires the incorpration of the surface response as well, which is the topic of the next section.

3.3 Holographic Surface Plasmon Polaritons

The key idea presented in the previous section is that by setting all sources s_μ to zero, we are demanding that the boundary theory satisfies Maxwell's equations,

with zero external current. This allows us to do more than just computing the n-point functions of the theory, and to consider other problems involving electromagnetism in a medium with strong correlations.

In addition to the bulk plasmon discussed in the previous section, there is also the possibility of exciting a collective electromagnetic mode that travels along the surface of a metal [118]. This is a surface plasmon polariton (SPP), where the appended 'polariton' refers to the fact that the induced wave also couples to the electromagnetic field outside of the metal. In the long-wavelength limit, the wave acquires a quasi-static character, where it is referred to only as 'surface plasmon'. The nature of SPPs are closely related to the dielectric function $\varepsilon(\omega, \boldsymbol{k})$ of the metal; for instance, the optical response will be proportional to $\mathrm{Im}(\varepsilon(\omega)+1)^{-1}$ [118]. Since the dielectric function also controls the behavior of the bulk plasmon, which behaves anomalously in strange metals, there is reason to believe that the same is true also for SPPs.

An important difference between SPPs and bulk plasmons is in the formulation of the typical setup. A bulk plasmon can be excited by inducing a perturbation of the electron density, where the resonance behavior is described by the density-density response function, shown in Fig. 3.1. As discussed in Section 3.1, the holographic framework is well-equipped for calculating Green's functions in the boundary theory, making the description of the bulk plasmon as a pole in the density-density correlator $\chi^{tt} = \langle \rho\rho \rangle$ straight-forward. SPPs, on the other hand, need to be excited by a very particular incoming electromagnetic wave and are not as easily formulated in terms of a Green's function.

In order to model SPPs, we consider a situation of an electromagnetic wave impinging on the surface of a strange metal, and use the reflection coefficient r (the ratio of the reflected and incoming waves' amplitudes) as the analogous response function for surface excitations [119]. In the non-retarded limit, relevant for the electrons in M-EELS experiments, it turns into the surface response function[11],

$$r \overset{\omega \ll ck}{\to} g(\omega, q) = \int_{-\infty}^{0} \int_{-\infty}^{0} \mathrm{d}z\, \mathrm{d}z' \chi(\omega, k; z, z') e^{|k|z} e^{|k|z'}, \tag{3.22}$$

which is closely related to the quantity measured in M-EELS experiments [48]. In the local $k \to 0$ limit, the surface response function reduces to the result $\mathrm{Im}\, g \to \mathrm{Im}(\varepsilon(\omega)+1)^{-1}$ obtained in optics.

The evaluation of the reflection coefficient involves either one of the displacement and magnetic fields, $\mathcal{D}$ and $\mathcal{H}$, which are related to the electric field $\mathcal{E}$ and magnetic flux density $\mathcal{B}$ as

$$\mathcal{D} = \mathcal{E} + \mathcal{P}, \quad \mathcal{H} = \mathcal{B} - \mathcal{M}. \tag{3.23}$$

[11] This is true for a p-polarized incoming wave [119].

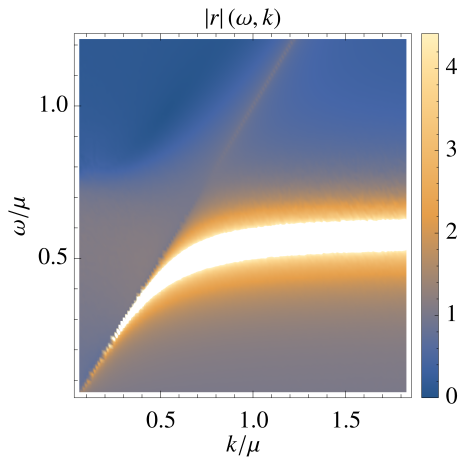

Figure 3.2: Absolute value of the reflection coefficient r as a function of the frequency ω and in-plane momentum k of the incoming electromagnetic wave, determined in a holographic RN model at $T = 0.02\mu$. The SPP is tangent to the light-line $\omega = k$ at small momenta, and settles at a finite frequency in the $k \to \infty$ limit.

In paper III, we show how the polarization $\mathcal{P}$ and magnetization $\mathcal{M}$ can be obtained in holographic models. This allows us to compute the reflection coefficient, and also provides access to the full permittivity (or dielectric function) $\varepsilon_{ij}(\omega, \boldsymbol{k})$ and permeability $\mu(\omega, \boldsymbol{k})$ of a holographic strange metal, via the constitutive relations $\mathcal{D} = \varepsilon\mathcal{E}$ and $\mathcal{B} = \mu\mathcal{H}$. Figure 3.2 shows the reflection coefficient r as a function of frequency ω and in-plane momentum k along the surface of the material. The SPP is tangent to the light-line $\omega = k$ for small momenta, and transitions into the electrostatic surface plasmon at a fix frequency ω_{sp} as $k \to \infty$.

Although the model presented in paper III, just like the bulk plasmon response discussed in the previous section, is too simplistic for a qualitative comparison with experimental data, it shows that a more complicated setup like that of an electromagnetic wave impinging on the surface material can in fact be formulated within the holographic framework. Together with the characterization of the dielectric function and the permeability, we can capture all of the electromagnetic properties of a strongly correlated system. By combining this work with the other studies on holographic plasmons, future research could provide a quantitative prediction of the plasmon response in strange metals.

Chapter 4

Summary and Outlook

The description of condensed matter systems is a daunting task. In this thesis, we have approached the problem from two very different viewpoints — one firmly rooted in Landau's quasiparticle description, and one that utilizes the exotic physics of black holes and the holographic duality.

The evolution of two-dimensional materials, combined with the developments in fabrication techniques, has enabled a hydrodynamic regime of electron transport to be experimentally realizable. This regime sits outside the realm of validity for typical perturbative approaches, and in this work, we have detailed a complete description of the interacting electrons in two-dimensional materials, that allows for a characterization of the electron liquid at all temperatures. Through the mathematical method presented in Chapter 2, there exists a host of response coefficients beyond the shear viscosity of paper I amenable to analysis, and all rely upon the solution to the electron-electron collision integral that we discuss in paper II. A logical next step is the inclusion of momentum dependence in the shear viscosity, as it controls signatures of hydrodynamics seen in experiments. Furthermore, due to the anomalously long-lived odd-parity modes seen in Fig. 2.3, it is particularly interesting to further investigate excitations that couple to the parity-odd modes, such as the momentum dependent part of the shear viscosity or the density-density response function. The full spectrum of modes obtained in paper II will also be important for thermal transport, which is sensitive to the higher-lying modes that cannot be obtained in self-energy calculations. Finally, further work could also extend the screened Coulomb interaction considered in Papers I and II to a more general interaction, that might be of importance in accurately describing the behavior near the Fermi temperature.

The intriguing behavior of strange metals has led to an interest in describing strongly correlated condensed matter systems using the holographic duality. In this process, essential features of real-world materials must be incorporated,

and we have in this thesis discussed one of them: the long-range Coulomb interaction. It gives rise to the collective modes known as plasmons, and at this point, the effect of many of the alluded features on the plasmon response have been considered in isolation [43–46, 105–108]. The field is therefore ripe for the construction of a model that combines all of the important aspects, in order to connect to the hitherto unexplained experimental data. We have contributed to this pursuit in the description of the surface response, which plays a role in the M-EELS experiments that provide a description of collective electronic excitations throughout momentum space.

Further holographic models of collective modes could investigate the so-called "Pines' demon", which was recently discovered in Sr_2RuO_4 [120], 67 years after its prediction by David Pines [121]. It is the charge-neutral out-of-phase superposition of two plasmon modes for two charge carrier species, and was found to exhibit a momentum dependence unexplained by current theory. Two charge carrier species can easily be implemented within a holographic model by including an additional gauge field, where the dynamical boundary conditions presented here will be key in obtaining the demon mode.

Finally, although certain aspects of Fermi surfaces have been incorporated into the holographic framework [86], it was recently argued that a key symmetry was missing, causing the Fermi surfaces of holography to not obey Luttinger's theorem [122]. Combining the proposed solution to this problem in [122] with a model of Coulomb interactions could perhaps be used to model a strongly correlated version of the Fermi surface deformations discussed in Chapter 2. As stated in the introduction, only through the exploration of physics at both ends of the 'Fermi liquid spectrum' might we be able to explain the phenomena in real systems, that feature elements of both Fermi liquid and non-Fermi liquid physics.

Bibliography

[1] D. Pines and P. Nozières, *The Theory of Quantum Liquids: Normal Fermi Liquids*, 1st ed., Vol. 1 (CRC Press, Boca Raton, 2018).

[2] L. D. Landau, "The Theory of a Fermi Liquid", Soviet Physics–JETP **3**, 920 (1957).

[3] A. C. Keser, D. Q. Wang, O. Klochan, D. Y. H. Ho, O. A. Tkachenko, V. A. Tkachenko, D. Culcer, S. Adam, I. Farrer, D. A. Ritchie, O. P. Sushkov, and A. R. Hamilton, "Geometric Control of Universal Hydrodynamic Flow in a Two-Dimensional Electron Fluid", Physical Review X **11**, 031030 (2021).

[4] J. Zaanen, "Planckian dissipation, minimal viscosity and the transport in cuprate strange metals", SciPost Physics **6**, 061 (2019).

[5] J. P. Reed, B. Uchoa, Y. I. Joe, Y. Gan, D. Casa, E. Fradkin, and P. Abbamonte, "The Effective Fine-Structure Constant of Freestanding Graphene Measured in Graphite", Science **330**, 805–808 (2010).

[6] M. Troyer and U.-J. Wiese, "Computational Complexity and Fundamental Limitations to Fermionic Quantum Monte Carlo Simulations", Physical Review Letters **94**, 170201 (2005).

[7] E. Y. Loh, J. E. Gubernatis, R. T. Scalettar, S. R. White, D. J. Scalapino, and R. L. Sugar, "Sign problem in the numerical simulation of many-electron systems", Physical Review B **41**, 9301–9307 (1990).

[8] E. Berg, S. Lederer, Y. Schattner, and S. Trebst, "Monte Carlo Studies of Quantum Critical Metals", Annual Review of Condensed Matter Physics **10**, 63–84 (2019).

[9] R. D. Mattuck, *A Guide to Feynman Diagrams in the Many Body Problem*, 2nd ed. (Dover Publications, New York, 1992).

[10] L. Fritz and T. Scaffidi, "Hydrodynamic Electronic Transport", Annual Review of Condensed Matter Physics **15**, 17–44 (2024).

[11] D. Wang, X.-B. Li, and H.-B. Sun, "Modulation doping: a strategy for 2D materials electronics", Nano Letters **21**, 6298–6303 (2021).

[12] J. Zaanen, "Electrons go with the flow in exotic material systems", Science **351**, 1026–1027 (2016).

[13] J. Crossno, J. K. Shi, K. Wang, X. Liu, A. Harzheim, A. Lucas, S. Sachdev, P. Kim, T. Taniguchi, K. Watanabe, T. A. Ohki, and K. C. Fong, "Observation of the Dirac fluid and the breakdown of the Wiedemann-Franz law in graphene", Science **351**, 1058–1061 (2016).

[14] R. Krishna Kumar, D. A. Bandurin, F. M. D. Pellegrino, Y. Cao, A. Principi, H. Guo, G. H. Auton, M. Ben Shalom, L. A. Ponomarenko, G. Falkovich, K. Watanabe, T. Taniguchi, I. V. Grigorieva, L. S. Levitov, M. Polini, and A. K. Geim, "Superballistic flow of viscous electron fluid through graphene constrictions", Nature Physics **13**, 1182–1185 (2017).

[15] D. A. Bandurin, A. V. Shytov, L. S. Levitov, R. K. Kumar, A. I. Berdyugin, M. Ben Shalom, I. V. Grigorieva, A. K. Geim, and G. Falkovich, "Fluidity onset in graphene", Nature Communications **9**, 4533 (2018).

[16] A. I. Berdyugin, S. G. Xu, F. M. D. Pellegrino, R. Krishna Kumar, A. Principi, I. Torre, M. Ben Shalom, T. Taniguchi, K. Watanabe, I. V. Grigorieva, M. Polini, A. K. Geim, and D. A. Bandurin, "Measuring Hall viscosity of graphene's electron fluid", Science **364**, 162–165 (2019).

[17] J. A. Sulpizio, L. Ella, A. Rozen, J. Birkbeck, D. J. Perello, D. Dutta, M. Ben-Shalom, T. Taniguchi, K. Watanabe, T. Holder, R. Queiroz, A. Principi, A. Stern, T. Scaffidi, A. K. Geim, and S. Ilani, "Visualizing Poiseuille flow of hydrodynamic electrons", Nature **576**, 75–79 (2019).

[18] A. Jenkins, S. Baumann, H. Zhou, S. A. Meynell, Y. Daipeng, K. Watanabe, T. Taniguchi, A. Lucas, A. F. Young, and A. C. Bleszynski Jayich, "Imaging the Breakdown of Ohmic Transport in Graphene", Physical Review Letters **129**, 087701 (2022).

[19] Y. Nam, D.-K. Ki, D. Soler-Delgado, and A. F. Morpurgo, "Electron–hole collision limited transport in charge-neutral bilayer graphene", Nature Physics **13**, 1207–1214 (2017).

[20] L. W. Molenkamp and M. J. M. De Jong, "Observation of Knudsen and Gurzhi transport regimes in a two-dimensional wire", Solid-state electronics **37**, 551–553 (1994).

[21] M. J. M. De Jong and L. W. Molenkamp, "Hydrodynamic electron flow in high-mobility wires", Physical Review B **51**, 13389–13402 (1995).

[22] A. Gupta, J. J. Heremans, G. Kataria, M. Chandra, S. Fallahi, G. C. Gardner, and M. J. Manfra, "Hydrodynamic and Ballistic Transport over Large Length Scales in GaAs / AlGaAs", Physical Review Letters **126**, 076803 (2021).

[23] G. M. Gusev, A. D. Levin, E. V. Levinson, and A. K. Bakarov, "Viscous transport and Hall viscosity in a two-dimensional electron system", Physical Review B **98**, 161303 (2018).

[24] G. M. Gusev, A. S. Jaroshevich, A. D. Levin, Z. D. Kvon, and A. K. Bakarov, "Viscous magnetotransport and Gurzhi effect in bilayer electron system", Physical Review B **103**, 075303 (2021).

[25] P. J. W. Moll, P. Kushwaha, N. Nandi, B. Schmidt, and A. P. Mackenzie, "Evidence for hydrodynamic electron flow in $PdCoO_2$", Science **351**, 1061–1064 (2016).

[26] J. Gooth, F. Menges, N. Kumar, V. Süß, C. Shekhar, Y. Sun, U. Drechsler, R. Zierold, C. Felser, and B. Gotsmann, "Thermal and electrical signatures of a hydrodynamic electron fluid in tungsten diphosphide", Nature Communications **9**, 4093 (2018).

[27] RN Gurzhi, "Hydrodynamic effects in solids at low temperature", Soviet Physics Uspekhi **11**, 255 (1968).

[28] B. Keimer, S. A. Kivelson, M. R. Norman, S. Uchida, and J. Zaanen, "From quantum matter to high-temperature superconductivity in copper oxides", Nature **518**, 179–186 (2015).

[29] J. Bardeen, L. N. Cooper, and J. R. Schrieffer, "Theory of Superconductivity", Physical Review **108**, 1175–1204 (1957).

[30] M. Gurvitch and A. T. Fiory, "Resistivity of $La_{1.825}Sr_{0.175}CuO_4$and $YBa_2Cu_3O_7$ to 1100 K: Absence of saturation and its implications", Physical Review Letters **59**, 1337–1340 (1987).

[31] P. W. Phillips, N. E. Hussey, and P. Abbamonte, "Stranger than metals", Science **377**, eabh4273 (2022).

[32] D. V. D. Marel, H. J. A. Molegraaf, J. Zaanen, Z. Nussinov, F. Carbone, A. Damascelli, H. Eisaki, M. Greven, P. H. Kes, and M. Li, "Quantum critical behaviour in a high-Tc superconductor", Nature **425**, 271–274 (2003).

[33] J. Zaanen, "Why the temperature is high", Nature **430**, 512–513 (2004).

[34] S. A. Hartnoll and A. P. Mackenzie, "*Colloquium* : Planckian dissipation in metals", Reviews of Modern Physics **94**, 041002 (2022).

[35] A. Legros, S. Benhabib, W. Tabis, F. Laliberté, M. Dion, M. Lizaire, B. Vignolle, D. Vignolles, H. Raffy, Z. Z. Li, P. Auban-Senzier, N. Doiron-Leyraud, P. Fournier, D. Colson, L. Taillefer, and C. Proust, "Universal T-linear resistivity and Planckian dissipation in overdoped cuprates", Nature Physics **15**, 142–147 (2019).

[36] S. Sachdev, *Statistical mechanics of strange metals and black holes*, 2022, arXiv:2205.02285.

[37] J. Zaanen, Y. Liu, Y.-W. Sun, and K. Schalm, *Holographic Duality in Condensed Matter Physics* (Cambridge University Press, Cambridge, 2015).

[38] F. Balm, N. Chagnet, S. Arend, J. Aretz, K. Grosvenor, M. Janse, O. Moors, J. Post, V. Ohanesjan, D. Rodriguez-Fernandez, K. Schalm, and J. Zaanen, "T-linear resistivity, optical conductivity, and Planckian transport for a holographic local quantum critical metal in a periodic potential", Physical Review B **108**, 125145 (2023).

[39] A. A. Patel, H. Guo, I. Esterlis, and S. Sachdev, "Universal theory of strange metals from spatially random interactions", Science **381**, 790–793 (2023).

[40] M. Mitrano, A. A. Husain, S. Vig, A. Kogar, M. S. Rak, S. I. Rubeck, J. Schmalian, B. Uchoa, J. Schneeloch, R. Zhong, G. D. Gu, and P. Abbamonte, "Anomalous density fluctuations in a strange metal", Proceedings of the National Academy of Sciences **115**, 5392–5396 (2018).

[41] J. Chen, X. Guo, C. Boyd, S. Bettler, C. Kengle, D. Chaudhuri, F. Hoveyda, A. Husain, J. Schneeloch, G. Gu, P. Phillips, B. Uchoa, T.-C. Chiang, and P. Abbamonte, "Consistency between reflection momentum-resolved electron energy loss spectroscopy and optical spectroscopy measurements of the long-wavelength density response of $Bi_2Sr_2CaCu_2O_{8+x}$", Physical Review B **109**, 045108 (2024).

[42] U. Gran, M. Tornsö, and T. Zingg, "Holographic plasmons", Journal of High Energy Physics **2018**, 176 (2018).

[43] A. Romero-Bermúdez, A. Krikun, K. Schalm, and J. Zaanen, "Anomalous attenuation of plasmons in strange metals and holography", Physical Review B **99**, 235149 (2019).

[44] S. T. Van Den Eede, T. J. N. van Stralen, C. F. J. Flipse, and H. T. C. Stoof, "Plasmons in a layered strange metal using the gauge-gravity duality", Physical Review B **109**, 085119 (2024).

[45] M. Baggioli, U. Gran, A. J. Alba, M. Tornsö, and T. Zingg, "Holographic plasmon relaxation with and without broken translations", Journal of High Energy Physics **2019**, 13 (2019).

[46] E. Mauri and H. Stoof, "Screening of Coulomb interactions in Holography", Journal of High Energy Physics **2019**, 35 (2019).

[47] U. Gran, M. Tornsö, and T. Zingg, "Holographic response of electron clouds", Journal of High Energy Physics **2019**, 19 (2019).

[48] A. A. Husain, "Charge Fluctuations of the Strange Metal in Space and Time", PhD thesis (University of Illinois at Urbana-Champaign, 2020).

[49] D. Arovas, *Lecture Notes on Thermodynamics and Statistical Mechanics (A Work in Progress)*, 2019.

[50] H Smith and H. H. Jensen, *Transport phenomena* (Oxford, 1989).

[51] J. A. McLennan, *Introduction to Non Equilibrium Statistical Mechanics*, 1st ed. (Prentice Hall, 1988).

[52] D. Tong, *Kinetic theory*, 2012.

[53] D. Jena, *Quantum physics of semiconductor materials and devices* (Oxford University Press, 2022).

[54] A. Altland and B. Simons, *Condensed Matter Field Theory*, 3rd ed. (Cambridge University Press, 2023).

[55] T. Kita, "Introduction to nonequilibrium statistical mechanics with quantum field theory", Progress of theoretical physics **123**, 581–658 (2010).

[56] H. J. Haug and A.-P. Jauho, *Quantum Kinetics in Transport and Optics of Semiconductors*, Vol. 123, Solid-State Sciences (Springer Berlin Heidelberg, Berlin, Heidelberg, 2008).

[57] J. Rammer, *Quantum transport theory* (CRC Press, 2018).

[58] J. Sólyom, *Fundamentals of the physics of solids* (Springer, 2007).

[59] A. A. Abrikosov and I. M. Khalatnikov, "The theory of a fermi liquid (the properties of liquid 3He at low temperatures)", Reports on Progress in Physics **22**, 329–367 (1959).

[60] G. A. Brooker and J. Sykes, "Transport Properties of a Fermi Liquid", Physical Review Letters **21**, 279–282 (1968).

[61] H. H. Jensen, H. Smith, and J. W. Wilkins, "Exact transport coefficients for a Fermi liquid", Physics Letters A **27**, 532–533 (1968).

[62] AV Chaplik, "Energy spectrum and electron scattering processes in inversion layers", Soviet Physics–JETP **33**, 997–1000 (1971).

[63] C. Hodges, H. Smith, and J. W. Wilkins, "Effect of Fermi Surface Geometry on Electron-Electron Scattering", Physical Review B **4**, 302–311 (1971).

[64] G. F. Giuliani and J. J. Quinn, "Lifetime of a quasiparticle in a two-dimensional electron gas", Physical Review B **26**, 4421–4428 (1982).

[65] L. Zheng and S. Das Sarma, "Coulomb scattering lifetime of a two-dimensional electron gas", Physical Review B **53**, 9964–9967 (1996).

[66] G. F. Giuliani and G. Vignale, *Quantum theory of the electron liquid* (Cambridge University Press, New York, 2005).

[67] G. B. Arfken and H.-J. Weber, *Mathematical methods for physicists*, 6th ed (Elsevier, Boston, 2005).

[68] T. Hahn, "Cuba—a library for multidimensional numerical integration", Computer Physics Communications **168**, 78–95 (2005).

[69] J. Hofmann and U. Gran, "Anomalously long lifetimes in two-dimensional Fermi liquids", Physical Review B **108**, L121401 (2023).

[70] S. Das Sarma and Y. Liao, "Know the enemy: 2D Fermi liquids", Annals of Physics **435**, 168495 (2021).

[71] J. J. Sakurai and J. Napolitano, *Modern quantum mechanics*, 2nd ed. (Cambridge University Press, Cambridge, 2017).

[72] P. J. Ledwith, H. Guo, and L. Levitov, "The hierarchy of excitation lifetimes in two-dimensional Fermi gases", Annals of Physics **411**, 167913 (2019).

[73] P. Ledwith, H. Guo, A. Shytov, and L. Levitov, "Tomographic Dynamics and Scale-Dependent Viscosity in 2D Electron Systems", Physical Review Letters **123**, 116601 (2019).

[74] M. Stephanov and Y. Yin, "Hydrodynamics with parametric slowing down and fluctuations near the critical point", Physical Review D **98**, 036006 (2018).

[75] S. Grozdanov, A. Lucas, and N. Poovuttikul, "Holography and hydrodynamics with weakly broken symmetries", Physical Review D **99**, 086012 (2019).

[76] J. Hofmann and S. Das Sarma, "Collective modes in interacting two-dimensional tomographic Fermi liquids", Physical Review B **106**, 205412 (2022).

[77] U. Gran, E. Nilsson, and J. Hofmann, *Shear viscosity in interacting two-dimensional Fermi liquids*, 2023, arXiv:2312.09977.

[78] M. Ammon and J. Erdmenger, *Gauge/Gravity Duality: Foundations and Applications* (Cambridge University Press, Cambridge, 2015).

[79] S. A. Hartnoll, A. Lucas, and S. Sachdev, *Holographic quantum matter* (The MIT Press, Cambridge, 2018).

[80] M. Baggioli, *A Practical Mini-Course on Applied Holography* (Springer, 2019).

[81] J. M. Maldacena, "The Large N Limit of Superconformal Field Theories and Supergravity", International Journal of Theoretical Physics **38**, 1113–1133 (1999).

[82] G. Compère and D. Marolf, "Setting the boundary free in AdS/CFT", Classical and Quantum Gravity **25**, 195014 (2008).

[83] A. Ishibashi, K. Maeda, and T. Okamura, "Semiclassical Einstein equations from holography and boundary dynamics", Journal of High Energy Physics **2023**, 212 (2023).

[84] G. T. Horowitz, J. E. Santos, and D. Tong, "Optical conductivity with holographic lattices", Journal of High Energy Physics **2012**, 168 (2012).

[85] L. Alberte, M. Ammon, A. Jiménez-Alba, M. Baggioli, and O. Pujolàs, "Holographic Phonons", Physical Review Letters **120**, 171602 (2018).

[86] M. Čubrović, J. Zaanen, and K. Schalm, "String Theory, Quantum Phase Transitions, and the Emergent Fermi Liquid", Science **325**, 439–444 (2009).

[87] H. Liu, J. McGreevy, and D. Vegh, "Non-Fermi liquids from holography", Physical Review D **83**, 065029 (2011).

[88] S.-S. Lee, "Non-Fermi liquid from a charged black hole: A critical Fermi ball", Physical Review D **79**, 086006 (2009).

[89] M. Tornsö, "Plasma Oscillations in Holographic Quantum Matter", PhD thesis (Chalmers University of Technology, 2021).

[90] E. Witten, *Anti De Sitter Space And Holography*, 1998, arXiv:`hep-th/9802150`.

[91] S. S. Gubser, I. R. Klebanov, and A. M. Polyakov, "Gauge theory correlators from non-critical string theory", Physics Letters B **428**, 105–114 (1998).

[92] P. K. Kovtun, D. T. Son, and A. O. Starinets, "Viscosity in Strongly Interacting Quantum Field Theories from Black Hole Physics", Physical Review Letters **94**, 111601 (2005).

[93] P. Romatschke and U. Romatschke, "Viscosity Information from Relativistic Nuclear Collisions: How Perfect is the Fluid Observed at RHIC?", Physical Review Letters **99**, 172301 (2007).

[94] M. Headrick, S. Kitchen, and T. Wiseman, "A new approach to static numerical relativity and its application to Kaluza–Klein black holes", Classical and Quantum Gravity **27**, 035002 (2010).

[95] M. Rangamani, M. Rozali, and D. Smyth, "Spatial modulation and conductivities in effective holographic theories", Journal of High Energy Physics **2015**, 24 (2015).

[96] J. P. Boyd, *Chebyshev and Fourier Spectral Methods* (Courier Corporation, 2001).

[97] P. M. Chesler and L. G. Yaffe, "Holography and Colliding Gravitational Shock Waves in Asymptotically AdS_5 Spacetime", Physical Review Letters **106**, 021601 (2011).

[98] P. M. Chesler and L. G. Yaffe, "Numerical solution of gravitational dynamics in asymptotically anti-de Sitter spacetimes", Journal of High Energy Physics **2014**, 86 (2014).

[99] A. Krikun, *Numerical Solution of the Boundary Value Problems for Partial Differential Equations. Crash course for holographer*, 2018, arXiv:1801.01483.

[100] S. Grieninger, "Non-equilibrium dynamics in Holography", PhD thesis (Friedrich-Schiller Universität Jena, 2020).

[101] S. A. Hartnoll, C. P. Herzog, and G. T. Horowitz, "Building a Holographic Superconductor", Physical Review Letters **101**, 031601 (2008).

[102] H.-S. Jeong, M. Baggioli, K.-Y. Kim, and Y.-W. Sun, "Collective dynamics and the Anderson-Higgs mechanism in a bona fide holographic superconductor", Journal of High Energy Physics **2023**, 206 (2023).

[103] M. Natsuume and T. Okamura, "Holographic Meissner effect", Physical Review D **106**, 086005 (2022).

[104] U. Gran, M. Tornsö, and T. Zingg, "Exotic holographic dispersion", Journal of High Energy Physics **2019**, 32 (2019).

[105] T. Andrade, A. Krikun, and A. Romero-Bermúdez, "Charge density response and fake plasmons in holographic models with strong translation symmetry breaking", Journal of High Energy Physics **2019**, 159 (2019).

[106] U. Gran, N. Jokela, D. Musso, A. V. Ramallo, and M. Tornsö, "Holographic fundamental matter in multilayered media", Journal of High Energy Physics **2019**, 38 (2019).

[107] U. Gran, M. Tornsö, and T. Zingg, "Plasmons in Holographic Graphene", SciPost Physics **8**, 093 (2020).

[108] M. Baggioli, U. Gran, and M. Tornsö, "Collective modes of polarizable holographic media in magnetic fields", Journal of High Energy Physics **2021**, 14 (2021).

[109] Y. J. Ahn, M. Baggioli, K.-B. Huh, H.-S. Jeong, K.-Y. Kim, and Y.-W. Sun, "Holography and magnetohydrodynamics with dynamical gauge fields", Journal of High Energy Physics **2023**, 12 (2023).

[110] M. E. Peskin and D. V. Schroeder, *An Introduction To Quantum Field Theory* (CRC Press, 2018).

[111] E. Mauri, "Applications of the gauge/gravity duality to the cuprate strange metal", PhD thesis (Utrecht University, 2022).

[112] J. Levallois, M. K. Tran, D. Pouliot, C. N. Presura, L. H. Greene, J. N. Eckstein, J. Uccelli, E. Giannini, G. D. Gu, A. J. Leggett, and D. van der Marel, "Temperature-Dependent Ellipsometry Measurements of Partial Coulomb Energy in Superconducting Cuprates", Physical Review X **6**, 031027 (2016).

[113] A. A. Husain, M. Mitrano, M. S. Rak, S. Rubeck, B. Uchoa, K. March, C. Dwyer, J. Schneeloch, R. Zhong, G. D. Gu, and P. Abbamonte, "Crossover of Charge Fluctuations across the Strange Metal Phase Diagram", Physical Review X **9**, 041062 (2019).

[114] J. Fink, *Comment on: Crossover of Charge Fluctuations across the Strange Metal Phase Diagram*, 2021, arXiv:2103.10268.

[115] A. Husain, M. Mitrano, M. S. Rak, S. Rubeck, B. Uchoa, K. March, C. Dwyer, J. Schneeloch, R. Zhong, G. D. Gu, and P. Abbamonte, *Reply to arXiv:2103.10268 'Comment on "Crossover of Charge Fluctuations across the Strange Metal Phase Diagram"'*, 2021, arXiv:2106.03301.

[116] M. Hepting, L. Chaix, E. W. Huang, R. Fumagalli, Y. Y. Peng, B. Moritz, K. Kummer, N. B. Brookes, W. C. Lee, M. Hashimoto, T. Sarkar, J.-F. He, C. R. Rotundu, Y. S. Lee, R. L. Greene, L. Braicovich, G. Ghiringhelli, Z. X. Shen, T. P. Devereaux, and W. S. Lee, "Three-dimensional collective charge excitations in electron-doped copper oxide superconductors", Nature **563**, 374–378 (2018).

[117] S. Vig, A. Kogar, M. Mitrano, A. A. Husain, V. Mishra, M. S. Rak, L. Venema, P. D. Johnson, G. D. Gu, E. Fradkin, M. R. Norman, and P. Abbamonte, "Measurement of the dynamic charge response of materials using low-energy, momentum-resolved electron energy-loss spectroscopy (M-EELS)", SciPost Physics **3**, 026 (2017).

[118] S. A. Maier, *Plasmonics: Fundamentals and Applications* (Springer US, New York, NY, 2007).

[119] A. Liebsch, *Electronic Excitations at Metal Surfaces* (Springer US, Boston, MA, 1997).

[120] A. A. Husain, E. W. Huang, M. Mitrano, M. S. Rak, S. I. Rubeck, X. Guo, H. Yang, C. Sow, Y. Maeno, B. Uchoa, T. C. Chiang, P. E. Batson, P. W. Phillips, and P. Abbamonte, "Pines' demon observed as a 3D acoustic plasmon in Sr2RuO4", Nature **621**, 66–70 (2023).

[121] D. Pines, "Electron interaction in solids", Canadian Journal of Physics **34**, 1379–1394 (1956).

[122] D. V. Else, *Holographic models of non-Fermi liquid metals revisited: an effective field theory approach*, 2023, arXiv:2307.02526.